Temperature-Dependence of the Contact Angle of Water on Graphite, Silicon, and Gold

Kenneth L Osborne III

A Thesis Submitted to the Faculty

of the

Worcester Polytechnic Institute

In partial fulfillment of the requirements for the

Degree of Master of Science

in Physics

April, 2009

APPROVED:

Dr. Rafael Garcia

Dr. Stephan A. Koehler

Dr. Alex A. Zozulya

Contents

Abstract

The temperature dependence of the contact angle of water on graphite, silicon and gold was investigated under various conditions to test the Sharp-Kink Approximation. Despite correctly predicting the contact angle at room temperature, the ideal Sharp-Kink Approximation was not found to accurately describe the contact angle's temperature dependence. The discrepancies from the predicted contact angle were characterized in terms of a correction H(T) to the liquid-solid surface tension. H(T) was found to be linear in temperature and decreasing, and is consistent with electrostatic charge effects.

Chapter 1

Introduction

This paper is the conclusion to a set of experiments taking place between December 2006 and November 2007. The purpose of the experiments was to make an initial study of the contact angle of water at room temperature and above. A hope was to reproducibly induce what is known as a 'wetting transition', a phenomenon wherein it becomes energetically more preferential for a droplet of liquid to spread out in a very thin layer instead of remaining in droplet form. This wetting transition is can be theoretically induced by increasing the temperature above a so-called 'wetting temperature'.

This paper surveys the math and physics that lead to the prediction of the wetting transition phenomenon, a phenomenon that manifests itself by abruptly changing the behavior of a bulk droplet of water at the wetting temperature T_w. Included in this survey are descpriptions of wetting vs non-wetting phenomenon and a tool, developed by Milton Cole [15] and recast in an especially simple form by Rafael Garcia [31], called the sharp-kink approximation.

Using the sharp-kink approximation it is possible to predict a contact angle for water on different substrates. Following the theoretical introduction to wetting and wetting transitions is a survey of recent research in the field, including papers that have used the sharp-kink approximation to accurately predict the contact angle, and thus demonstrating its validity. The survey of recent research also serve to present the methods used in past experiments. Then there an overview of the experimentation done in this paper will be presented.

1.1 Theory of Wetting and Wetting Transitions

The experiments reported on in this paper examine droplets that are small enough that capillary effects are negligible. Such small droplets, look like small truncated spheres when placed on the surface of a substrate. Given a droplet of a liquid of constant volume, a sphere's height off The truncated spheres form an angle with the substrate at the liquid-substrate interface, which is known as the 'contact angle'. The equations predicting contact angle require knowledge of the surface tensions at the liquid-gas interface σ_{lg}, the surface tension at the solid-liquid interface σ_{sl}, and the surface tension at the gas-solid interface σ_{gs}. Because σ_{sl} and σ_{gs} have yet to be determined for most interfaces, including all such interfaces utilized in this experiment, it is hard to predict the contact angle based on this theory.

Thus, until relatively recently when Cole et al published their paper [15] on the sharp-kink approximation it was almost impossible to predict the behavior of contact angles. The sharp-kink approximation predicts the contact angle from just the liquid-gas surface tension σ_{lg}, the difference in density between the liquid and vapor, and the van der Waals potential describing the net preference of the adsorbate water for wetting the substrate instead of forming a droplet. This preference is determined from equations modeling intermolecular forces.

After study, it is found that the sharp-kink approximation upholds qualitatively the long-standing prediction that there is a 'wetting temperature' T_w, which varies depending on the three surface tensions at the three pairs of interfaces. Above the theoretical T_w a water droplet will have a contact angle of zero degrees [15]. The sharp-kink approximation has be experimentally validated by predicting pre-wetting transitions at low temperatures [2], but the theory has not been tested at room temperature. As such, this experiment was done to test the validity of the sharp-kink approximation at room temperature, by testing if the sharp-kink approximation correctly predicts the contact angle of water on graphite and gold.

1.1.1 Thin Films and Contact Angles

One of the assumptions that is made about the system is that there is only a microscopically thin film of liquid which adsorbs on the surface of the substrate. This thin film is assumed for the purposes of this experiment to be of 1-2 layers uniform thickness and moreover is uniformly present everywhere on the substrate. This is different than the bulk-like liquid droplet which is localized to a small section of the substrate.

At the place where the three interfaces (liquid, vapor, and solid surface with thin film) meet, called the 'three-phase contact line', or TCL, the water-air interface forms an angle with the substrate, see Figure 1.1. This angle, called the contact angle is an observable manifestation of the interactions of the three surface tensions.

Depending on the contact angle the droplet is characterized as completely wetting, non-wetting, or completely non-wetting. Figure 1.2 shows droplets in

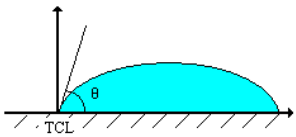

Figure 1.1: The ring around the droplet where liquid, vapor and solid surfaces meet is called the TCL. At the TCL the droplet makes a contact angle θ with the substrate.

all three stages of wetting. When a liquid is wetting a surface, the liquid has a 0 degree contact angle. Furthermore the droplet spontaneously spreads out in a thin sheet on the substrate surface.

When a liquid is completely not wetting a substrate, a droplet the liquid rests on top of the substrate, with a 180 degree contact angle at the three-phase contact line. A side view shows that the completely non-wetting droplet looks like an untruncated sphere resting on the substrate surface.

The intermediate case is the that where the droplet is partially wetting the surface. This is the case where the contact angle is above 0 but less than 180 degrees at the three-phase contact line. The droplet looks like a sphere that has been truncated, resting on top of the substrate.

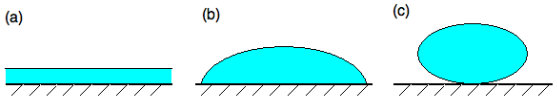

Figure 1.2: a) The droplet has completely wet the substrate, and hence, is spread across the surface of the substrate and has a contact angle of 0 degrees. b) The droplet is not wetting the surface, but the contact angle is still less than 180 degrees. c) The droplet rests on the surface of the substrate with the liquid-solid interface at an angle of 180 degrees with respect to the substrate surface. The droplet looks like a sphere on the surface of the substrate.

1.2 van der Waals Potential

The van der Waals potential describes the attraction of individual molecules the substrate that they are resting on, and to other molecules. In the specific case where V is a Lennard-Jones 3-9 potential, with a well depth D and a van der Waals coefficient C, the van der Waals Potential is given as

$$V(z) = \frac{4C^3}{27D^2z^9} - \frac{C}{z^3} \tag{1.1}$$

Here $V = V_s - V_l$ describes the net preference of the adsorbate molecule for wetting the substrate instead of forming a droplet, due to intermolecular forces. In the definition of V, V_s is the potential energy of the adsorbate molecule due to the substrate and V_l is the potential energy of the adsorbate molecule due to a hypothetical puddle of bulk liquid at the same location as the substrate. These terms include both attractive van der Waals forces and repulsive forces that result from the excluded volume of the adsorbate molecule, as seen in Figure 1.3.

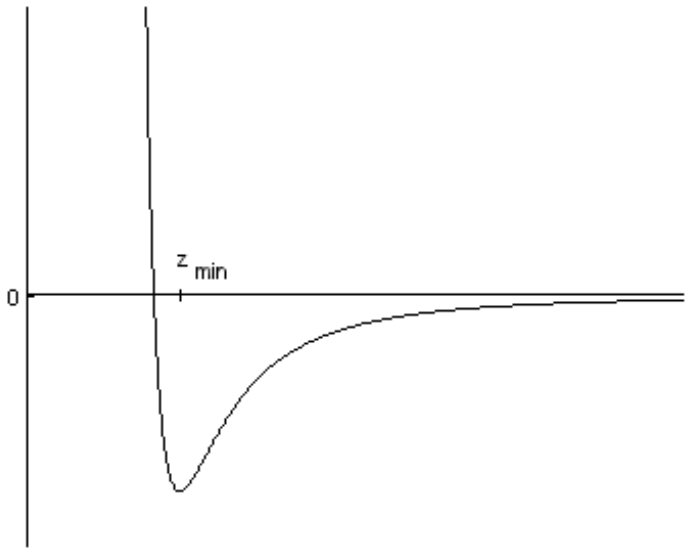

Figure 1.3: A 3-9 van der Waals potential. When D is sufficiently large, there is a minimum in the energy graph at z_{min}. The radius r of a molecule is comparable length corresponding to the forbidden section of the van der Waals potential in the sharp kink approximation.

The integral is taken over the thickness of the droplet starting from the minimum of the van der Waals potential of the near the surface z_{min}. This is done because z_{min} is assumed to coincide with the position of the first layer of molecules on the surface. The thickness of the bulk droplet is assumed to be infinite, because it is a great number of atomic lengths away.

From the equation for $V(z)$ it is possible to find the distance from the substrate surface at which water molecules will adsorb. Setting $dV/dz = 0$ shows that $z_{min} = (2C/3D)^{1/3}$. After having solved for z_{min} we can now integrate $V\,dz$ in order to find $I = 0.600\left(CD^2\right)^{1/3}$. In accordance with the sharp-kink approximation, the first layer of atoms coincides with the minimum of V, which is a good approximation whenever D is sufficiently deep that atoms

behave as they would in the classical limit.

1.3 The Sharp Kink Approximation

Under the saturated vapor-pressure conditions discussed in Thin Flms and Contact Angle, the contact angle θ is related to the surface tensions on the gas-solid, gas-liquid, and liquid-solid layers by the Young Eq. 1.2

$$\sigma_{gs} = \sigma_{ls} + \sigma_{lg} \cos\ \theta \tag{1.2}$$

This equation is only valid in the case where the droplet is not completely wetting the substrate. An equivalent form that is more useful is

$$\sigma_{ls} - \sigma_{gs} = -\sigma_{lg} \cos\ \theta \tag{1.3}$$

A large problem with this equation is that σ_{gs} and σ_{ls}, and their temperature-dependences, in general, cannot be determined experimentally. At present, there has only been one experiment [] to independently determine all four parameters in Eq. 1.2. The van der Waals potential models the attraction of individual atoms in the bulk liquid, and their attraction to the substrate. In a moment it will be shown that the difference $\sigma_{ls} - \sigma_{gs}$ can be modeled by integrating the van der Waals potentials of all atoms in the bulk liquid

The 'sharp-kink' approximation assumes that the atoms that reside at the minimum energy of the van der Waals potential form the first layer of liquid atoms of the liquid layer. This assumption showed to be a good approximation by Dietrich [9] because the radius of an atom is comparable to the distance z_{min}, which means that the first layer of atoms in the droplet almost touches the layer of atoms on the substrate.

A typical van der Waals 3-9 potential is shown in Figure 1.3. The potential has an excluded region, that atoms are classically forbidden from entering. Beyond the excluded region is z_{min}, the minimum of the potential. Classically, the atoms would start to fill this potential at the point, and as filling continued, some of the atoms would fill part of the classically forbidden space as seen in Figure 1.4 (top) [31].

To simplify the problem, we assume that the atoms fill the van der Waals potential like Figure 1.4 (bottom) shows that ρ sharply changes from its ρ_g to ρ_l at z_{min} [31]. The actual density profile shows that density is only fractionally greater than the bulk density z_{min}, and beyond a few atomic radii away, the density of atoms that would fill a van der Waals matches the bulk density. This shows Dietrich's approximation to be sensible.

Cole et al [15] noticed that if the above approximations were made about $\Delta\rho$, then σ_{sl} could be broken into three different sections, as shown in Figure 1.5. In the Figure the substrate and liquid are separated by a distance z_{min} which is greater than the radius of an atom, while there is a gas section between.

Cole et al used Dietrich's descriptions of the sharp-kink approximation to show that σ_{ls} can be thought of as a system in which there is a thin layer of gas

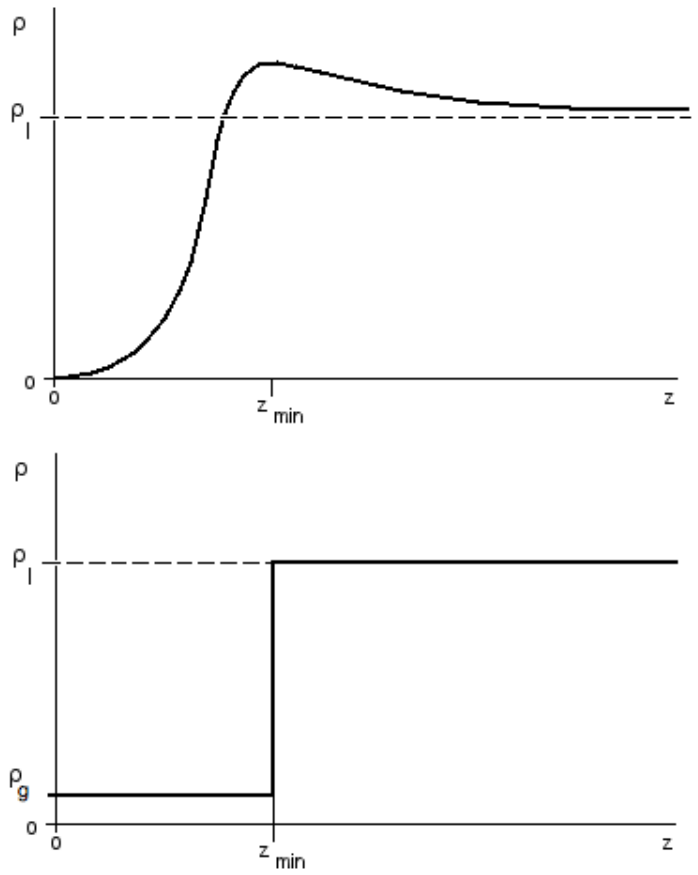

Figure 1.4: (top) Calculated density profile in a van der Waals 3-9 potential [9]. (bottom) Density profile using the sharp kink approximation [9]. The sharp-kink approximation also assumes ρ is does not vary with distance, and remains at the bulk value beyond z_{min}.

between the solid and liquid interface. Thus, the entire liquid-solid boundary can be thought of as having three distinct energies: a solid-gas surface tension, a liquid-gas surface tension, and a third quantity that adds the van der Waals attraction of the liquid to the substrate in order to compensate for the fact that the liquid has a different density than the gas layer. The sharp-kink approximation in this form further assumes that the liquid-vapor interface that exists between the liquid and solid has a negligible width.

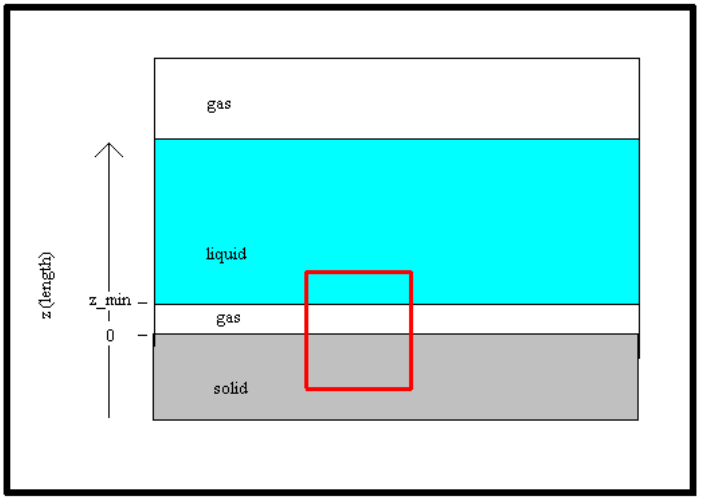

Figure 1.5: The sharp-kink approximation assumes the solid-liquid surface tension is the surface tension of the solid-gas interface and a liquid-solid interface and a quantity that compensates for the fact that the liquid has a different density than the gas layer [15].

Based on the heuristic explanation given above and with help from Figure 1.5 Cole *et al* draw the conclusion

$$\sigma_{ls} \approx \sigma_{gs} + \sigma_{lg} + \Delta\rho \int_{z_{min}}^{\infty} V(z)\, dz \tag{1.4}$$

V, the van der Waals potential is described in further detail in the Section entitled van der Waals Potential.

We can rewrite Eq. 1.4 to put the $\sigma_{ls} - \sigma_{gs}$ onto one side of the equation. Once this is done, we may equate this to Eq. 1.6, and solve for cos θ, where $I = -\int_{z_{min}}^{\infty} V(z)\, dz$, the negative of the van der Waals integral. From here on, I will be referred to as the van der Waals integral for brevity.

$$\begin{aligned}\sigma_{gs} - \sigma_{ls} &= \sigma_{lg} \cos\ \theta \\ &= -\sigma_{lg} - \Delta\rho \int_{z_{min}}^{\infty} V(z)\, dz \qquad (1.5)\\ \cos\ \theta &= -1 + \frac{\Delta\rho}{\sigma_{lg}} I \qquad (1.6)\end{aligned}$$

The cases of special interest occur when θ is 0 or 180 degrees. These cases are interesting because they allow us to confirm the value of the van der Waals integral based on the behavior of the contact angle. Wetting occurs when $\theta = 0$ degrees, or alternatively, when $\cos\ \theta = 1$. Thus, according Eq. 1.6 above T_w the liquid-vapor surface tension σ_{lg} is predicted to be

$$2 \leq -\frac{\Delta\rho}{\sigma_{lg}} \int_{z_{min}}^{\infty} V(z)\, dz \qquad (1.7)$$

In the complete non-wetting limiting case, $\theta = 180$ degrees, and $\cos\ \theta = -1$. Thus, the complete non-wetting limiting case will occur when

$$\frac{\Delta\rho}{\sigma_{ls}} \int_{z_{min}}^{\infty} V(z)\, dz \leq 0 \qquad (1.8)$$

This criterion can be filled only when $\Delta\rho/\sigma_{ls} = 0$ or $V(z) = V_l - V_s \leq 0$. If $\Delta\rho/\sigma_{ls} = 0$, then the bulk liquid has the same density the vapor surrounding it, whereas, if $V(z) \leq 0$, it is energetically more preferential for the droplet to form a sphere than spread over any part of the substrate surface.

Both σ_{lg} and $\Delta\rho$ are dependent on temperature, and both of these quantities go to zero as $T \to T_c$. This is because near T_c the liquid and vapor phases become indistinguishable from one another. Hence, to determine the behavior of the contact angle from our equation, we need to determine the limiting behavior of the fraction $\frac{\Delta\rho}{\sigma_{lg}}$ tends to T_w from the negative side, which we denote $T_c{}^-$. It is known that $\Delta\rho$ and σ_{lg} follow power laws of the form

$$\Delta\rho \propto \Delta\rho_0\, t^{\beta} \qquad \sigma_{lg} \propto \sigma_{lg_0}\, t^{\gamma} \qquad (1.9)$$

where $t = \left|\frac{T_c - T}{T_c}\right|$ and $\beta \approx 0.31$, $\gamma \approx 1.24$. It is clear from both the power law behavior that $\frac{\Delta\rho}{\sigma_{lg}}$ tends to ∞ near $T_c{}^-$.

By assuming that the van der Waals potential changes very little over the range of temperatures used during experimentation, Eq. 1.6 shows that the temperature-dependence of $\cos\ \theta$ is the temperature-dependence of $\frac{\Delta\rho}{\sigma_{lg}}$. Thus, because $\frac{\Delta\rho}{\sigma_{lg}} \to \infty$ at T_c^-, it is expected that $-1 + \frac{\Delta\rho}{\sigma_{lg}} \to 1$ and thus $\theta \to 0$ at some $T_w < T_c$. Because the contact angle θ is abruptly changing from a non-zero value to a zero value at the wetting temperature T_w, we say that the contact angle undergoes a wetting transition.

Now that the basics of wetting transitions has been explained, we're going to back-track and examine the van der Waals

1.4 Experiment

In this paper we report a number of experiments that examine the behavior of contact angle vs temperature of droplets of water on different substrates. The experiments commenced at room temperature, and continued up to 130 °C. The experiment surveyed the contact angle of water on three different substrates: graphite, silicon, and gold. We studied water on graphite and gold because other experiments have studied the contact angle of water on these substrates, thus results from this experiment can be compared with other experiments for consistency. We studied water on silicon because water has a small contact angle on silicon at room temperature. Because the sharp-kink approximation decreases monotonically with increasing. Thus it is expected that water will wet the substrate at temperatures much greater than room temperature. This will be the first experiment to examine the temperature-dependence of the contact angle.

As the first experiment to study the temperature-dependence of contact angle, this experiment was able to test the temperature-dependence of the sharp-kink approximation. The experiment tested the validity of the sharp-kink approximation by comparing experimentally obtained values of contact angle against values calculated using Eq. 1.6. As yet, Eq. 1.6 had not been experimentally tested, furthermore no experiments that have directly observed the contact angle of water at room temperatures. Instead similar experiments have relied on resonant vibrations of a quartz micro-balance [4], [5].

The experiments monitored contact angles by photographing a droplet of water as temperature is increased. The temperature of the droplet of water was monitored by a thermometer, thus allowing temperature to be compared with contact angle.

Having thus laid out the proposed experiment in its basic form, the Methods section will now explain the experimentation process in greater detail.

Chapter 2

Methods

The methods of carrying out the experiments and analyzing the photographs are very intricate, with a lot of special cases. Because this research is an initial look at the temperature-dependence of change in contact angle, the methods that were changed regularly to examine and understand new facets of wetting that happened in previous experiments.

There are three aspects that the methods section will cover: Preparation, Experimentation, and Image Processing. Each of these three methods changed throughout the course of the research, and changes in methodology are marked in the Results section as well.

2.1 Preparation

There are three major components to explain about cell preparation: The Cell, Preparing the Droplet, and Cleaning the Cell.

In the section entitled 'The Cell' the cell's parts are described. There are qualitative and quantitative descriptions of the cell, as well as descriptions of why the cell was built in this way.

'Preparing the Cell' outlines how and why the cell was constructed. It goes on to describe the standard experimentation preparation procedure that we recommend for use during future experimentation studying the relationship between contact angle and temperature. Finally it describes the range of different procedures for preparing the droplet used during experimentation.

'Cleaning the Cell' describes the products and techniques used to make sure the cell was pristine and ready for droplet preparation. This is important because during experimentation the cell is placed in a bath of silicone oil, and experimental results might be invalidated if the silicone oil contaminated the cell.

2.1.1 Cell Parts

This experiment deals studies the contact angle's dependence on temperature. As such, temperature must be controlled. We chose to control the temperature by immersing the cell in a controlled temperature silicone oil bath, which will be discussed in Section 2.2.2.

The cell is constructed mostly out of stainless steel, which holds the droplet, substrate, and reservoir during experimentation (these three items will be further discussed in Preparing the droplet). The purposes of the cell are: to provide a pristine environment, to keep silicone oil and other impurities out, to allow the optical observation of droplets from the side, and to sustain high pressures caused by heating a body at a fixed volume without letting particles in or out.

The cell is comprised of 13 parts. The biggest part of the is the 'T' shaped cell body. The part is produced by Swagelok and is part number SS-8-VCO-T. The top of the stainless steel 'T' is 6.4 cm long, 2.1 cm long, and 2.1 cm wide. The bottom part of the 'T' is 4.3 cm long and 2.1 cm wide. The inside of the 'T' is hollowed out as well. The pieces are hollowed out in the shape of a circle with cross-section 1.25 cm in diameter.

On each side of the three sides of the cell body goes four parts. The first thing that goes onto each side of the cell body is a Teflon O-ring. These O-rings are provided by McMaster Carr, part number 111TEF. The three Teflon O-rings fit into O-ring slots, one on each end of the cell body. The reason we chose to use these O-rings is that Teflon could withstand the range of temperatures studied during experimentation, whereas the three Bruna-N O-rings that came with the cell body could not withstand the entire temperature range. Furthermore, teflon O-rings were used because the experiments never reached temperatures high enough to justify switching to metal C-rings, which are of superior quality, but are much more expensive and one time use.

On each Teflon O-ring is placed a cylindrically shaped sapphire window. The windows allowed for viewing of the droplet. By having a window on each side of the cell, it was possible to light the droplet from the back, as well as to see the droplet from outside the cell. A backlit droplet has the benefit of having a droplet that looks very different than it's background. This benefit was exploited to determine the contact angle of the droplet of water. The sapphire windows were procured from Meller Optics, item no. MSW075/125Z. The windows are 0.750 inches in diameter, and 0.125 inches thick. The diameter was chosen to fit onto the end of the cell body, and the thickness was enough so that the windows would not crack under the heat and pressure range of the experiment.

The last piece that goes on the cell body to complete the cell is the cell cap. The cell cap fits down over the other pieces, and screws onto the cell body. When the cell caps are tightened the cell is impervious to the outside environment. The piece is produced by Swagelok, part number: SS-8-VCO-4. The cell caps are hexagonally shaped and 2.25 cm across. The inside of the cell cap acts as a nut that fits onto the cell body, and has a diameter of 2.06 cm. The cell cap has a 1.56 cm diameter circular hole in the side, which enables droplet viewing.

Before the cap is tightened an aluminum O-ring is placed between the sap-

phire window and the cell cap. The aluminum O-ring spreads out the pressure of the cell cap over a greater surface area on the sapphire window, making it less likely that the sapphire window would crack. The aluminum O-ring has the further benefit of shielding the sapphire windows from the stainless steel cell cap as it is tightened by turning. The aluminum O-rings were made by folding in two a sheet of aluminum foil, and cutting out O-rings that had an outer diameter less than than 2.06 cm, and an inner diameter less than 1.56 cm (these being the dimensions of the inside of the cell cap).

Together and assembled, these pieces make up the cell in which the experiment takes place. The next section will explain how the cell is assembled and how the droplet is prepared for experimentation.

2.1.2 Preparing the Cell

The cell assembly did not change throughout the course of the experiment, and thus will be discussed first.

The aspects of the procedure of preparing the cell which most varied was how the details of how the substrate, reservoir, and droplet were added to the cell. Depending on the experiment, the droplet of water varied in volume, composition, purity, and charge. The substrate was either silicon, graphite, or gold. The size, composition and purity of the reservoir of water within the cell were also varied throughout experimentation, although the composition and purity of the reservoir of water always matched that of the droplet. The final parameter that was varied throughout experimentation was the grounding of the cell.

After the cell parts have been cleaned the cell is partially assembled. Next the substrate, reservoir and droplet are added to the cell, and when this is complete, the cell is sealed and ready for experimentation. Next the standard procedure for preparing the droplet is discussed, and lastly the deviations from the standard procedure are discussed. The procedure for cell assembly is explained in the next section.

Cell Assembly in General

The cell was most efficiently assembled by putting together all the parts of the cell that could be put onto the cell before adding the substrate, reservoir, and droplet, and then carefully finishing the assembly. This section will explain how the initial and final assembly was done, while leaving the minutiae of adding the substrate, reservoir, and droplet to another section.

The cell was always assembled in a clean-room, in front of a laminar flow hood to prevent contamination. The assembler always wore a gown and hair cover made of 100% Height Density Polyethylene, in addition to booties to keep dirt from shoes from contaminating the clean room environment.

First, three Teflon O-rings are (forcefully) inserted into the three ends of the cell body. Next, two of the sapphire windows are put on the sides of the cell body. Of the two sides selected, one should be the bottom of the 'T' of

the cell body, and the other should be one of the sides. Next all three cell caps should have aluminum O-rings placed on the inside. Next two cell caps should be tightened onto the two sapphire windows. This was usually done by hand tightening the cell caps (with aluminum rings inside) onto the two sapphire windows. After hand tightening, the cell was placed in a vice grip, and the cell caps were tightened with a wrench. This was done to feel, and was an art; too much pressure would crack the window, and too little pressure resulted in the cell not being sealed.

After tightening two sides, the substrate, reservoir, and droplet were added to the cell. This is described in detail in the next section.

Finally, the last window was put on, and the last cell cap, with aluminum O-ring inside, was tightened onto the cell. This final procedure could not be done by placing the cell in a vice grip as before because the cell needed to be kept level in order to keep the water from the reservoir off of the substrate and windows (the water can become pinned to the windows, obscuring visibility). Instead, a different method for closing the cell involving two people was used. The final cell cap was initially hand-tightened and then tightened with two adjustable wrenches. One wrench was placed on the cell while the second was placed on the hand-tightened cell cap, and the wrenches were spun in opposing direction to close the cell. While the cell was being sealed with wrenches, a second person stood still, holding the cell and keeping it level. After the cell was sealed in this way, it was ready for experimentation.

Standard Procedure for Assembling the Cell

Throughout the course of experimentation, several changes were made to the procedure of putting the substrate, reservoir and droplet into the cell. The procedure that provided the best result is chronicled here, and deviations from the standard procedure are marked in later sections.

After the cell had both end caps sealed, the cell was put on a stand made out of aluminum foil. This stand made the cell tilt backwards just slightly. First the substrate was added to the cell. There were three substrates that were used during experimentation: graphite, silicon, and gold. One of these three was selected, and the selected substrate was slid into the cell. Moving the substrates was done by using a pair of clean tweezers to hold the edge of the substrate. Moving was done in this way because the droplet was much less likely to be placed on a corner of the substrate than on any other part.

In the cell, the substrate was situated so that the section of the substrate that was closet to the open end of the cell was 1.2 ± 0.3 cm from the open end of the cell. This location was chosen because it was found that when the experiment was happening, temperature gradients in the cell near the windows caused condensation. The further away from the windows the substrate was, the more uniform the temperature was across the substrate, and the less likely it was that condensation would occur on the substrate due to the gradients. However there is a tradeoff, pushing the substrate further away from the window also meant that the droplet would appear to be smaller, resulting in a greater

uncertainty in contact angle. Thus, it was found that about 1.2 cm from the window maximized droplet size while stopping condensation from occurring.

After the substrate was placed, the reservoir of water was added to the cell. The standard water used had a resistivity of 18.2 MΩ-cm to match that of the droplet to be added later. The water was ordered from the Ricca Chemical Company, cat. no. 9150-5 and had a resistivity of $\geq$ 18.2 MΩ-cm upon shipping. This water was then filtered through an Easy Pure II, made by Barnstead. The standard reservoir size was 400μL, and the standard location was directly under the substrate. It was found that a 400μL reservoir would help deter evaporation of the droplet as the cell temperature was varied, and wouldn't cause problems with water pinning to the cell windows. When water became pinned to the cell windows, the droplet was invisible, or at least, partially obscured. The reservoir was placed directly under the substrate using a pipette. This was done to help saturate the air near and around the substrate with water vapor. The droplet would eventually be on the substrate, and so surrounding the droplet with already humid air helped deter evaporation.

For the next ten to twenty minutes the cell cap would be hand tightened onto the cell, and the reservoir, air in the cell, and substrate were allowed to equilibrate. This means that the water would slightly evaporate into the cell's air, and small amounts of water vapor would adsorb on the surface of the substrate. The initial contact angle became slightly more controlled by allowing the reservoir and substrate to equilibrate in this way.

After allowing the reservoir and the substrate to equilibrate, the hand-tight cell cap was removed, a $1.0 \pm 0.1\mu$L droplet of water was placed on the substrate inside the cell using a pipette. The water used in the reservoir was the same as the water used for the droplet. 3 - 5 seconds after placing the droplet onto the substrate, the cell was sealed by reaffixing the cell cap as described in the section Cell Assembly.

Variations in Procedure

Variations to the standard procedure described above were made during different experiments. Several minor differences were noted in the results section as they changed from one experiment to the other. For the purposes of this paper, a minor difference is a difference that doesn't fundamentally change the nature of the experiment, and may be described in one line. Such differences include droplet size, reservoir size, droplet location, substrate location and equilibrium procedure.

But there were other times, when the experiment was modified to examine several facets of water in addition to studying temperature-dependence of the contact angle of water. Such facets included examining whether the relationships between droplet volume, purity, saturation conditions, and charge as a function of droplet contact angle.

Droplet volume, purity, and saturation conditions will be discussed here and droplet charging is given its own section below because it is a complex discussion topic.

Droplet volume was varied between some experiments in order to try to create a droplet that wouldn't evaporate entirely during experimentation. On a similar note, the location of reservoir that was used to saturate the air with water in order to prevent droplet evaporation was found to be optimal when the reservoir was directly below the substrate. By modifying these parameters, droplet evaporation was minimized.

Droplet resistivity was varied between experiments as well. The water used in early experiments had been filtered to 17.5 MΩ-cm several months prior to experimentation, but it was suspected that this water had since become less pure. New sources of water were used in order to try to eliminate variations in experimental results due to impurities in the water. Though there are issues beyond simple droplet purity. In early experiments, fully prepared cells were left to sit in the bath of silicone oil overnight, in order to equilibrate before taking experimental data. It was later found that leaving the cell in the oil overnight may have allowed for small amounts of oil to leak into the cell. The oil impurity could have dramatically changed the results of many experiments, and should therefore be carefully scrutinized. Later experiments were not allowed to sit in the silicone bath overnight in order to minimize contamination.

Explaining Charging Effects

During some experiments, the cell was discharged by connecting it to a ground. The reason this is done was that it was suspected that droplet and cell charging might be adversely impacting experimental results.

To discharge the cell, we first completely constructed the cell as described in the standard procedure (with any minor variations described in the experiment). Then the cell was removed from the clean room and held by a person wearing Microflex Free Form SE Nitrile Powder free gloves. The person would wrap a wire around the cell, so that one loop of exposed copper was wrapped around the cell. Next, an exposed piece of the opposite end of the wire was wrapped around a tap with cold water pouring through it. Thus the water flowing through tap and the cell were brought to the same potential, because there was very little resistance between the two objects.

The description of discharging the cell above was realized to have the fault of assuming that the water running through the taps was neutrally charged, so another experiment removed this assumption. In the follow-up experiment the water used for both the reservoir and droplet were mixed with NaCl. The solution was 60 g of water to 1 g of salt. The water and salt were swirled together in a glass jar and the resulting mixture was substituted with the purified water in the standard procedure section. The saltwater solution was used because salt has the property of neutralizing charges. With such a strong concentration with salt in the saltwater, the resulting reservoir and droplet were both very close to neutrally charged.

The only problem with the latter experiment was that it was studying salt water, which had a higher contact angle than purified water. The data obtained from the experiments was still useful though, because according to the theory,

the only thing that really matters is the shape of the curve that was made from changing the temperature over time. The shape of the saltwater curve could provide insight about purified water.

A final experiment was done to test the effect of charging on contact angle. In this experiment, the cell was intentionally charged before experimentation. To do this, the cell was prepared in the standard procedure, and then set upon some aluminum foil near an air purifier. An electroscope was used to measure that an air purifier emitted charge. By placing the cell on aluminum foil in front of the air purifier, it was certain that the cell would become charged. After 45 minutes of letting the cell become charged, tongs wrapped with electrical tape were used to move the cell into place for experimentation.

2.1.3 Cleaning the Cell

After each experiment the cell is removed from the silicone oil and cleaned. The cell is cleaned to prevent contaminations which may have adverse effects on later experiments.

The cell was first rinsed with warm water until the silicone oil has left the surface of the cell. After the exterior was clean, adjustable wrenches were used to open one side of the cell.

What happened next depended on the substrate. One piece of graphite substrate was very expensive, and thus used throughout the entirety of experimentation. Because of this, the graphite needed to remain uncontaminated, and as such was extricated from the cell in the clean room. The graphite substrate was removed from the cell by tilting the cell slightly and using clean tweezers to grab one corner of the graphite. The graphite was then pulled out of the cell and placed in a clean aluminum box. The water was emptied from the cell into a garbage can and the cleaning of the cell continued.

If the substrate was silicon, after the cell was opened the substrate and water were emptied into a garbage can. The silicon substrates were less expensive and so a new piece of silicon substrate was in every experiment.

In the one experiment where gold was studied, the substrate was kept because the gold substrate was prepared by experimenters for potential future use. The gold substrate was kept because it was made in the lab and took a lot of effort to make. It was removed from the cell in the same way the graphite was removed.

After removing the substrate from the cell, the rest of the cell was disassembled and placed on a piece of clean aluminum foil. The aluminum and teflon O-rings were thrown away for several reasons. First of all they weren't very expensive, next they seemed to get silicone oil on them from experimentation, finally the teflon O-rings couldn't be cleaned with the high power cleaning reagent acetone because acetone evaporates teflon.

At this stage, the remaining pieces of cell to be cleaned were the cell body, three cell caps, and three sapphire windows. Each of these was rinsed with water until no more silicone oil was left on any piece. After this initial rinsing, each piece was covered in hand-soap, scrubbed, and then rinsed. The hand-soap

cleaning was done three times with each piece. After being rinsed, the pieces were set onto a new clean piece of aluminum foil.

The hand-soap leaves a fragrant residue, and so each of the seven pieces was washed with the cleaner Alconox three times. Alconox is a blend of sodium linear alkylaryl sulfonate, alcohol sulfate, phosphates, and carbonates. It was ordered from VWR Scientific Products, VWR Catalog No.: 21835-032. Alconox comes in a powder, and so a pipe cleaner with large bristles coming out of it was used to hold a little of the powder from the Alconox container in its bristles. The piece was flushed with water and scrubbed with the newly soaped pipe cleaner.

After every piece was washed with alconox three times, the pieces were then rinsed in three different liquids three times, and then any excess liquid was blown off the piece. So first a piece was rinsed with acetone three times, then the same piece was rinsed with methanol three times, then the piece was rinsed in watered filtered to a resistivity of 17.5 MΩ-cm three times. After being rinsed the piece was blown dry using the compressed gas Dust-Off. Dust-off was applied until there were no visible droplets left on the piece. The piece was then set on a clean piece of aluminum.

Acetone was used because it is chemical cleaner devoid of unnecessary perfumes. Methanol was used for the same reason. Water was then applied to rinse away any of the buildup that had been stored in the methanol. Water was also chosen because it had the added benefit of evaporating much slower than methanol. This was important because if the liquid containing contaminants evaporated, then the contaminants would be placed back on the piece. To prevent this happening, the final liquid that was on a piece was relatively slowly evaporating liquid water, and Dust-Off was applied to the water remaining on the piece, blowing off any contaminants with the water.

Using the Dust-Off to blow excess liquid off the pieces was the final step in cleaning the cell. After this, the cell was ready for reassembly in the clean room.

2.2 Experimentation

This section gives a brief overview of how the experiment works, and what parts are used, followed by a detailed description of what techniques were used and why.

2.2.1 Overview

Experimentation involved putting the constructed cell in an oil bath, controlling the temperature of the bath, and taking pictures of the droplet sealed inside the cell while this was going on. To the outside of the cell was lashed a platinum thermometer, which monitored the temperature of the bath.

A lamp connected to a variable AC transformer, or variac, was set to produce a proper amount of backlighting behind the droplet to optimize droplet visibility. A CD camera was mounted to a telescope so as to see the droplet inside the cell. A program called camstream captured images from the CCD camera at a user specified rate (usually 1 image every 5 minutes).

2.2.2 Detailed Description

There are two independent operations that are going on in this experiment: temperature control and imaging. The two function almost independent of one another and so will be described in two different sections below.

Cell Placement

The sealed cell with droplet, substrate, and reservoir inside, was held level with a pair of tongs and lowered into the bath. The bath was a tank of silicone oil, whose function will be described fully in the Temperature Control section of this report. At the bottom of the tank, the cell was placed upon a large piece of aluminum. After the cell was securely placed on the aluminum, it was visually confirmed that the droplet was still in its proper location. After visual human confirmation, it was time to make the droplet visible to the recording the droplet during experimentation.

The camera used was a Philips 1/3 inch VGA CCD camera. In video mode, the mode that we used to run experimentation, the camera ran in 640 x 480 resolution. A telescope, placed between the CCD camera and the droplet, was used to achieve an optical zoom. This magnified the droplet so it filled more of the camera's field of view, an important part of accurately and precisely determining a droplet's contact angle. More information about why a larger droplet is important can be found in the image processing section under error analysis.

After the cell had been placed in the silicone oil, we needed to make the camera see the droplet. To do this, the cell was pushed around the tank with prongs until the droplet was in sight. After the droplet was in sight, the droplet needed to be fully visible, and in focus. Adjusting the focus was done second

since making the droplet fully visible changed the focus point location. It was necessary to make the droplet fully for several reasons, the most important part of which is that the base of the droplet (typically the hardest part to see) is the point from which the contact angle is calculated. The rest of the droplet should be visible in order to determine the contact angle with greater accuracy, see image processing for more details.

The ideal droplet is one viewed from the side, with the camera aligned perfectly with the edge of the substrate. The closer one is to this ideal situation, the more a droplet looks like truncated circle, which, in turn, causes the best contact angle calculations. This ideal case is unattainable because it is very important to see where the droplet contacts the surface of the substrate. If there is a slight tilting backward so the place where the droplet contacts the substrate cannot be seen, then photographs will be unable to show the correct contact angle. Conversely, if the substrate is tilted too far forward, then the droplet no longer looks like a truncated sphere, and the algorithm to calculate the droplet's contact angle does not apply. Therefore, it was settled that the substrate should be tilted forward just far enough to see the place where the droplet contacted the substrate. This made the contact angle calculations less accurate, but was much more accurate that not seeing the place where the droplet met the substrate.

The substrate was tilted by tilting the entire cell. The cell was tilted by placing packets of folded aluminum foil under the cell caps, using tongs and a screwdriver to nudge the cell into place relative to the camera.

When the droplet was manipulated into the position described above, the camera and microscope objective were adjusted so as to focus on the droplet. The camera and microscope objective were mounted to one another on a rail. To adjust the focus, we changed the position of the mount on the rail.

After the droplet was in focus, a lamp behind the tank was manipulated to illuminate the droplet. The lamp was flexible and was bent into location. The variac, which was connected to the lamp, was then adjusted to a brightness that would make the droplet look much darker than the rest of the background. This was done for image processing purposes. Sometimes the background wasn't bright enough, and images needed to have the space behind the droplet removed in order to determine the contact angle. This is discussed further in image processing.

With the camera and lamp in place, the program camstream was set to take a still image from the CCD camera at a rate of 1 image per 5 minutes. Additional pictures were taken if the cell needed to be adjusted or if it was suspected that a wetting transition might occur. As pictures were being taken, the temperature was being increased. In this way, it was possible to extract the contact angle of a droplet on a substrate as a function of temperature.

Temperature Control

Before the cell was put into the silicone oil bath, a platinum thermometer was attached to it. The cell was then lowered into the silicone oil bath and adjusted

as described above. After the camera started taking pictures, the thermometer was used to record the temperature of the cell. The temperature inside the cell was lower than the temperature recorded by the thermometer throughout duration of the experiment. This was because the heat needed to permeate through the cell walls and windows before it changed the conditions around the droplet, and it took time to have the heat permeate through.

A glass tank holds inside silicone oil inside it. and tubes running to and from a temperature controller. The temperature controller was a Neslab RTE-111 temperature controlled bath, BOM Number: 134103212606. The oil was heated to a set-point that was set by a human about once per hour. It took a while to heat the entire bath, thusly the initial set point was much higher than the temperature monitored by the thermometer. At the beginning of experimentation, the thermometer was typically reading room temperature (24 ± 2°C), while the initial set point on the temperature controller was 65 or 70 °C. As the temperature increased according to the platinum thermometer, the set point was likewise increased.

During early stages of experimentation, the rate of temperature change was much slower than later experiments. In the first experiment, for example, the temperature changed 90°C over the course of 8 hours, or an average of 11.25°C per hour. In later experiments, the temperature rate of change was much quicker, with some experiments spanning 90°C in 4 hours. The switch was made to a larger change in temperature per unit time because it seemed that faster experimentation did not change experimental results. As an additional benefit, more data could be collected in the same amount of time under the new paradigm.

The temperature was controlled to ever higher temperatures until one of the following occurred: the temperature controller gave out, the droplet was noticeably evaporating, the droplet disappeared from view, or until it was suspected that the cell might be contaminated if experimentation continued. The vast majority of cases presented above have been discussed in this Methods chapter, or in the Results chapter, and therefore do not require further explanation. The exceptions are the cases when the temperature controller 'cut-out'.

Sometimes, at high temperatures, the Neslab temperature controller would turn itself off and not let itself be turned back on again until its heater had cooled to a sufficient temperature. This safety feature posed a problem when seeking to study the behavior of the droplet at temperatures above 100°C. The high temperature cut-out and the tendency of the droplet to evaporate at high temperatures severely hindered the scope of experimentation. Further studies might make use of a more robust temperature controller when controlling to temperatures above 100°C.

2.3 Image Processing

The overall objective of the image processing section is to create a program to determine the contact angle of a droplet resting on a substrate. This objective

is broken into three tasks.

1. Image Preparation. The image processing section includes all image preparation, such as turning the image into a set of zeros and ones, image cropping or image rotation. Most of the image processing is done early in the program.

2. User Input. During the program the user is asked to provide human input. The user is to identify the location where the droplet contacts the substrate. This user input because it easier for a human to see the actual points decide than to determine by only computer logic.

3. Mathematical Manipulation. While the first two categories send initial data to the computer, the task of mathematical manipulation acts as a stand-alone, almost independent from the rest of the program. It takes data (in this case provided by image processes and user input) and determine the contact angle.

The basic idea is that a small droplet resting on a substrate looks like part of a sphere. A partial sphere viewed from the side looks like a partial circle. Furthermore the substrate, the medium on which the droplet is resting, looks like a line. It is possible to determine the two angles between a line and a circle. Therefore, it was necessary to obtain equations describing the location of the droplet and the substrate from a picture, with the assumption that a droplet could be mathematically described as a circle, and the substrate could be described as a line. A method was found for making the droplet stand out, and then a circle was fit to the region that stood out. User inputs provided the so called 'substrate surface', the line where the substrate touches the droplet.

2.3.1 Image Preparation

Image processing manipulates the image to facilitate data acquisition during both the user input and the mathematical manipulation sections. The first steps that the program does are primarily image processing. The program initially smoothes the back ground, which has the effect of highlighting the droplet and its reflection as in Figure 2.2. After highlighting has taken place the droplet needs to be described by a circle. This requires the picture to be transformed into data.

The most important notion taken from Matlab was the ability to do a so-called 'binarization'. This means that Matlab can take a picture and turn it into an array consisting of only zeros and ones. Figure 2.3 provides an example of an image before and after binarization. Turning a the picture with the highlighted droplet into a set of binary data allows for more subtle forms of analysis. The highlighted section was turned white in order to get the portion of the image with the droplet and reflection separate from the rest of the picture.

Next the picture is cropped to remove any reflection off of the substrate and rotated to put the substrate at the bottom of the screen 2.4. The cropping

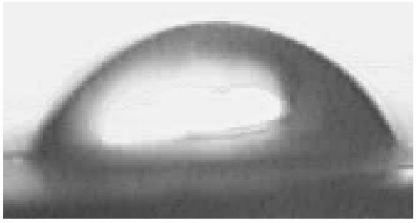

Figure 2.1: This is the original image file taken in by the Matlab program and converted to black and white. This image will be manipulated, and from it the contact angle of the droplet will be extracted.

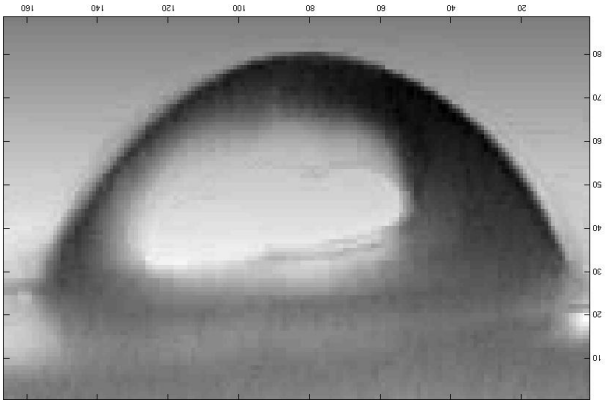

Figure 2.2: The image back ground has been smoothed when compared the back ground in Figure 2.1. This has the effect of highlighting the droplet and its reflection.

Figure 2.3: After smoothing the back ground the program binarizes the image. This means that the picture is turned into a set of black and white points which can be mathematically analyzed.

Figure 2.4: After binarizing the image, all back ground noise from the picture is removed. The bar of data that didn't belong in Figure 2.3 is removed during this step.

and rotation are done based on user inputs described in the user input section. After the image thus prepared the circle that best fills the white area, and thus the circle that best represents the droplet is found through mathematical interpretation. As a final check, the program shows a picture of the white area representing the droplet superimposed with a picture of the circle that was found to best fit the white area. An example of such a picture can be found in Figure 2.5.

Figure 2.5: In Figure 2.4 the program mistakes some of the droplet as background. This error is correct by filling in all black regions contained within a white region.

2.3.2 User Input

User input is utilized because determining the places where a droplet contacts its corresponding substrate are much easier for a human to determine than to determine by some scheme involving only computer logic. User input is required in only one step: identifying the so-called 'contact points'. Contact points are two points where the droplet stops looking like a circle, and contacts the substrate. The user identifies these two points to the program by clicking the left and right contact points on the black and white picture described during image processing. Figure 2.6 shows a user clicking on two contact points. The program stores the points as x_{left} and x_{right}. These points will be used as inputs for image processing and mathematical manipulation.

Figure 2.6: A user clicks the three-phase contact line at the left and right sides of the droplet in the figure above.

2.3.3 Mathematical Manipulation

This section is describes how the contact angle of a droplet is mathematically determined. It is important to note that after all data have been gathered, the data interpretation objective. This means that there is no mathematical uncertainty in the resulting contact angle. The only uncertainties lie in the data gathered, and the assumptions made. In this interpretation, the assumption is that the contact angle is determined to be the angle between a line, and a circle. Physically this means the contact angle at the three-phase contact line is represented by the angle between the substrate and the droplet, respectively.

The major mathematical steps are

1. Determine the equation for the substrate surface. The substrate surface is the place where the droplet touches the substrate.

2. Determine the equation of the circle that best resembles the droplet.

3. Determine the contact points. The contact points are given as the locations where the circle and line intersect one another.

4. Determine the contact angle. The contact angle is found to be the angle between the slope of the circle at the points of intersection and the slope of the line.

This is important because it may be slightly different than the contact points found in step 1 due to the fitting that occurs in step 2.

Substrate Surface

This section determines the equation of the substrate surface. The substrate surface is found through interpretation of two data points supplied by the user. Here the data are called (x_{left}, y_{left}) and (x_{right}, y_{right}). The slope of the line connecting these two points is given by Eq. 2.1.

$$m = \frac{y_{left} - y_{right}}{x_{left} - x_{right}} \tag{2.1}$$

It was stated in the image processing section that to make subsequent calculations easier, the picture is rotated to make the substrate appear flat. Given m, the angle through which the picture must be rotated is given by

$$\theta = -tan^{-1}(m) \tag{2.2}$$

The negative sign is introduced to show rotation in the direction opposite to the existing contact angle.

The two points may be determined to lie on a unique line by setting the data into point slope form. Here the left point is arbitrarily chosen as the point of reference.

$$y - y_{left} = m(x - x_{left}) \tag{2.3}$$

Equation of the Circle

The image with which this section is most strongly connected is that of where the droplet has been turned into data using binarization and cropped to removed reflections. This image will be referred to as the data image in this section.

A circle can be fit to the the white area in the data image. A function was created to give quality ratings to circles that attempt to represent the partial circle found in the data image. The quality function has the property that the lower the score, the better the quality. First the function draws a circle at a specified starting location. The function then examines two categories. The first category is the overlap between the drawn circle and the white area in the data image, this is labeled 'good'. The second category is the overlap between

the drawn circle and the black area, this is labeled 'bad'. The function then gives the quality value

$$value = \frac{1}{|good - bad|} \tag{2.4}$$

The purpose of the quality function is to be minimal when the drawn circle maximally overlaps the white circle, and minimally overlaps any black area. Next the quality function is given to the function 'fminsearch(fun,x_0)'. This fminsearch(fun,x_0) function starts at the point x_0 and finds a local minimum x of the function described in fun. x_0 can be a scalar, vector, or matrix. fun is the name of a function. In this case x_0 is a vector that details the radius and center of a circle to be drawn. The local minimum x then uniquely specifies the optimal circle to describe the white area; its center ($x_{center} = x_0, y_{center} = y_0$) and radius r_0 are logged.

Contact Points

The next objective is to find the location of the three-phase contact line. This is achieved by finding the where the contact points. On the mathematical level this is equivalent to finding where the circle and line intersect.

In general the equations a line and circle are

$$y - y_{left} = m(x - x_{left}) \tag{2.5}$$
$$(x - x_0)^2 + (y - y_0)^2 = {r_0}^2 \tag{2.6}$$

But during the image processing the picture was rotated to make our line flat and at the bottom of the picture. This corresponds to the line

$$y = B \tag{2.7}$$

where B is the y-intercept. Notice there is no x dependence in this equation

Substituting Eq. 2.7 into Eq. 2.6 yields the equation for an intersection of a line and a circle

$$(x - x_0)^2 + (B - y_0)^2 = {r_0}^2 \tag{2.8}$$
$$x^2 - 2x_0x + {x_0}^2 + (B - y_0)^2 = {r_0}^2 \tag{2.9}$$
$$x^2 + 2x_0x + (B - y_0)^2 + {x_0}^2 - {r_0}^2 = 0 \tag{2.10}$$

Parameters a, b, and c are introduced in order to simplify Eq. 2.10. They are chosen to reduce Eq. 2.10 to a standard quadratic.

$a = 1$, $b = 2x_0$, and $c = \left[(B - y_0)^2 + {x_0}^2 - {r_0}^2\right]$. Thus changing our expression to

$$ax^2 + bx + c = 0 \tag{2.11}$$

The quadratic has a solution of the form

$$x = -\frac{b}{2a} \pm \frac{\sqrt{b^2 - 4ac}}{2a} \tag{2.12}$$

These two solutions will be called x_1 and x_2. Corresponding y_1 and y_2 can be found by substituting x_1 and x_2 into Eq. 2.6.

Eq. 2.14 displays the final from of the x the x coordinates of the points of intersection between any arbitrary line and a circle.

$$x = -\frac{2x_0}{2} \pm \frac{\sqrt{(2x_0)^2 - 4(1)\left[(B - y_0)^2 + {x_0}^2 - {r_0}^2\right]}}{2} \tag{2.13}$$

$$x = -x_0 \pm \sqrt{\frac{x_0^2}{2} - \left[(B - y_0)^2 + {x_0}^2 - {r_0}^2\right]} \tag{2.14}$$

The y-coordinate of the intersection is given as $y = B$ by Eq. 2.7.

Contact Angle

With the location of the contact points determined, one can combine all collected data and thus determine the contact angle of a droplet on a substrate.

The slope of the tangent to a curve at any given point is given by the derivative at that point. Using implicit differentiation, we know the slope of the line tangent to a circle is given by

$$\frac{d}{dx}\left((x - x_0)^2 + (y - y_0)^2\right) = \frac{d}{dx}({r_0}^2) \tag{2.15}$$

$$2(x - x_0) + 2(y - y_0)y' = 0 \tag{2.16}$$

$$y' = -\left(\frac{x - x_0}{y - y_0}\right) \tag{2.17}$$

Where $y' = dy/dx$ is the equation of a line tangent to a circle at the contact points (note: not the line). Plugging in for (x_1, y_1) and (x_2, y_2) gives the slope of the line tangent to the circle at the corresponding points.

The angles between the slope of the line tangent to the circle y' and the slope of the substrate surface $m = 0$ are the contact angles. For ease of calculation, both slopes are converted into vector format. The vectors represent the changes corresponding to taking a step of unit length in the $\pm\hat{x}$ direction from contact points (x_1, y_1) and (x_2, y_2). At the left contact point, the step is taken in the $+\hat{x}$ direction and at the right contact point the step is taken in the $-\hat{x}$ direction. Thus the vectors that describe the tangents to the droplet (at the contact points) and the substrate given by

$$\vec{v_1} = [y'(x_1, y_1)\ 1] \tag{2.18}$$

$$\vec{v_2} = [0\ 1] \tag{2.19}$$

$$\vec{v_3} = [y'(x_2, y_2)\ 1] \tag{2.20}$$

$$\vec{v_4} = -[0\ 1] \tag{2.21}$$

The angle between vectors $\vec{v_1}$ and $\vec{v_2}$ gives the left contact angle, and the angle between vectors $\vec{v_3}$ and $\vec{v_4}$ gives the right contact angle. The expression for the angle between two vectors is

$$\theta = \cos^{-1}\left(\frac{\vec{u_1} \cdot \vec{u_2}}{||\vec{u_1}||\ ||\vec{u_2}||}\right) \tag{2.22}$$

Using the four supplied vectors it is possible to determine the two contact angles.

2.3.4 Program Code for Determining Contact Angles

The latter sections detailed the general method of how a program determines the contact angle of a droplet on a substrate at the three-phase contact line. This section describes in-depth the actual program and what it's doing, every step of the way.

Before describing program implementation, a few notes on writing structure are in order. The code is broken into separate tasks. Each task acts as a piece of information separate from the rest of the code. All major image processing changes are marked with new figures, e.g. figure(1), and are terminated with some function that calls for the image to be displayed, e.g. imshow, imagesc. The purpose of displaying an image at the end of each section was to aid the user in following the image processing changes made to the pictures by the program.

The Main Program runs through a list of tasks, with each task building on the information from the previous tasks. The program is, in this way, comprised of twelve individual tasks that are necessary for calculating the contact angle of a droplet on a substrate.

Initializing the Program

The first task is to initialize the program. This involves calling the image that had been prepared for analysis, and closing all windows that may be open. A grayscale version of the original image is displayed on the screen.

Convert to Gray

Next a new window is opened, and in it is displayed a grayscale version of the image created in when initializing the program. Additionally, the image is changed to from a regular 'img' type, to the type 'double'. This is in preparation for later on: only images of type 'double' may be converted to binary images.

Remove Background Noise

To remove the background noise it is necessary to have the computer recognize the droplet and the background as two distinct objects. The first portion of this task was to create as uniform a background as possible, so as to highlight the droplet from the rest of the picture. The idea here is to create an image that resembles the non-uniform background. By subtracting this noise from the standard image, a the background is made more uniform. This normalized background image was created by using the information at the corners. In order

to create an accurate background image, the four pixels nearest to each corner were used. The mean intensity of the four pixels closest to each corner defines the intensity value at that corner to be used in the image named 'background'. The values of grayscale intensity near the corners of the image sampled, and these values are given in Matlab by the lines

```
im(1:2,1:2),im(1:2,end-[0:1],im(end-[0:1],1:2),im(end-[0:1],end-[0:1])
```

The meshgrid takes the mean values of each corner and interpolates values intermediary values. After determining how many values should be interpolated in each direction, the meshgrid values are saved in the image named 'background'. In the program, the size of the meshgrid as based on the size of the original picture. The size of the original picture was stored in the values a.inp, b.inp, a.out, and b.out. The background picture was also defined in size by a.inp, b.inp, a.out and b.out, making the original picture and the background picture the same size. Next, the interpolated background data was subtracted from the original image to create a 'corrected' image. The corrected image is the final result of the task one with a more uniform background. The image is then displayed on a grayscale. Without this function it would be much harder to clearly define what is an edge, and what is not. The meshgrid interpolated smooth transitions between the intensity values at each corner. The interpolated image was then named 'background'.

Black and White Image

This task transforms the corrected image, that highlighted the droplet, into binary data. This data is later used to extract the contact angle at the three-phase contact line. In this step the water droplet is not only highlighted; for the first time it is set apart from the rest of the data. From a programming perspective, section 'figure(3)' changed the corrected image from figure(2) into a black and white image, 'BW'. This was done using im2bw. The 0.02 appearing in the im2bw function was an adjustable parameter. This parameter could be set to different values in order to make to adjust the intensity above which an individual pixel turns white.

Identify Droplet

To identify the droplet in the picture, the program identified regions of the picture that could be droplets. These were regions where there were a lot of white points clustered together. An assumption was made that the largest white region defined the droplet. All regions that weren't a member of the largest region were then identified as noise, and were therefore removed. Thus the data is refined to be only from the region believed to be the droplet.

All the data in figure(3) was searched through for the region that could be the droplet. Within this data 'L' labeled all the regions that were contiguous. Contiguous regions were defined as being one of the four closest squares to each other piece of data, e.g. directly to the left, right, above or below another piece of the remaining data. The labeling is done using the function bwlabeln. the size 'S' of each labeled region was then found with the regionprops function. Finally the largest region is then determined by using a combination of the

ismember, find, and max functions. The ismember gives out an input of true or false. The code was then configured to delete all data that's not part of the largest section, and thus, not part of the droplet. The resultant image is then displayed as figure(4).

Fill in Droplet

The previous task filtered external noise, but section six filters noise within the droplet. The internal noise results from parts of the droplet that didn't stand out very much and were subsequently assumed to be non-droplet area. The droplet image data was then restored using the imfill command. The image figure(5) displays the doctored droplet.

Identify Substrate

In this task the user is called upon to input data during the program. The user interaction plays an integral role in droplet image processing. As can be seen in IMAGE Y a reflection of the droplet on the substrate cannot be distinguished from the image of the original droplet. This reflection occurs along the substrate surface. Identifying this line is crucial for determining the contact angle. Contact angles are measured with respect to this substrate surface. Furthermore substrate surface is not easy to determine by computer logic. The program is based on a human's ability to input the left and right edges of the water droplet. The coordinates of the information received were put into two vectors: x_coordinates and y_coordinates. This was done using the impixel function. The impixel function also displays the intensity of the pixel selected, but this information is not used.

Prepare for Circular Fitting

The first action undertaken to prepare for the circular fitting was to develop an equation representing the substrate surface. The y-intercept and the angle that the substrate surface makes with respect to the edge of the picture are stored. After obtaining this information it is possible to remove the reflection image from the rest of the image, leaving only the actual droplet. First the image is truncated to the level of the substrate surface. Next the image was rotated to make the substrate surface flush with the bottom of the picture. The image, figure(6), is then displayed. From this state it is very easy to determine the contact angle.

Initialize Circular Fit

Task nine initializes the circular fitting process, discussed in the section entitled 'Equation of the Circle'. The program looks at two special functions 'fit_fun' and 'circle', that have parameters corresponding to the location of the center of a circle, as well as BW4, the matrix representation of figure(6). From these parameters the special function 'circle' draws an initial circle, centered at (200,300) with initial radius 250. The special function 'circle' will be discussed in depth in task 13. 'fit_fun' then examines the overlap between the circle drawn with 'circle', and the white region from BW4. 'fit_fun' determines a quality value based on how much the drawn circle overlaps the white region, and how little the drawn circle overlaps the black region. A circle that corresponds to the data well has a lower quality value.

Fit Best Circle

This task finds finds the best-fit circle that matches the black and white droplet image. The circle is fit by finding the lowest possible quality value, and recording the corresponding center and location of the circle. The lowest possible quality value is determined using the Matlab function fminsearch. In this case, the variable 'cntr_radius' is a vector comprised three components. These components correspond to the center of the circle (both x and y) and the radius of the circle. As will be explained in further detail later, fit_fun gives a quality value that will be minimal when the drawn circle best resembles the white region in the image BW4.

Display Confirmation Picture

After determining the equation for the best-fit circle, this section displays an image to confirm that the fitting worked. The optimized circle is made into an image and then overlayed with the original picture. The two images can be simultaneously viewed using the function imagesc. In order to distinguish the original image from the fitted image, the values of the fitted image is multiplied by ten, making the fitted image appear red in figure(7).

Calculate Contact Angles

Task twelve does the actual contact angle calculation. The contact angle is calculated by finding the angle between the vectors tangent to the circle and the substrate surface. The technical details for understanding task twelve require a bit of geometry, and not just programming. Please refer to the section entitled Mathematical Manipulation for further reference. To calculate the contact angles it is necessary to know vectors $\vec{v_1}$ - $\vec{v_4}$. The tangent to the circle at the contact points must be calculated in order to know $\vec{v_1}$ and $\vec{v_3}$. The contact points are given as the points where the circle intersects with the line. From Eq. 2.14

$$x = -x_0 \pm \sqrt{\frac{x_0^2}{2} - [(B - y_0)^2 + {x_0}^2 - {r_0}^2]} \tag{2.23}$$

the x-coordinates are known. Here x_0 and y_0 represent location of the center of the circle, and r_0 represents the radius of the circle. Notice it is not necessary to find the y-coordinate, because after making the substrate surface flush with the bottom of the picture, the equation for the y-intercept is given by $y = 1$. In the program these coordinates are stored as the vector 'contact_pt'. The slope of line tangent to the circle is given by Eq. 2.17.

$$y' = -\frac{contact\_pt(1) - x_0}{contact\_pt(2) - y_0} \tag{2.24}$$

Where x_0 and y_0 again represent location of the center of the circle.

With y' thus determined at the contact points it is possible to construct the vectors $\vec{v_1}$ and $\vec{v_3}$. The contact angle is calculated in radians. Multiplying by $\frac{180}{\pi}$ converts the contact angle to degrees.

The final step is to make sure the angles correspond to the coordinate in the proper quadrant. Inverse trigonometric functions can detail information about the location of a point in only two quadrants. To correct for the discrepancy, it is necessary to use the mod function.

The corrected contact angle is the last line that the program executes, which would cause the program is to be complete. However, two special functions were created. These functions were not 'in line' commands, and so were functions added to the end of this program below the 'return' line. Although the functions have task numbers thirteen and fourteen, they do not occur in that order. The functions are called when needed, and after completing a task, each function returns to the line of the program from which it left.

The first special function was named 'circle' and it created an image with fitted circle points. The function draws a circle at a specified location on a background of specified size. The function 'circle' requires inputs that define the radius, location of the center of a circle, and an image.

First the function specifies the bounds of the area on which drawing is to occur. This is defined to be from -radius to +radius. The domain is then further restricted to be circular. Next a matrix of zeroes defines the background based on the size of the input image. Finally the bounded circular domain is placed in the location entitled center within the matrix. All the points within this circle are turned white while the rest of the circle remains black. The function circle outputs a matrix that has a circle at a pre-specified location with a pre-specified radius of a pre-specified image size.

The second function that I made was a determined the so called 'quality' of a circle as a fitting figure of merit.

Task fourteen defines the special function 'fit_fun'. This function compares a picture with a drawing and determines a quality value based on similarities between the two. The quality value goes down as the similarities increase. 'fit_fun' requires inputs that define the radius, location of the center of a circle, and an image.

The first thing 'fit_fun' does is create a mock circle, by calling the other special function 'circle'. 'circle' returns a matrix of a circle. Next 'fit_fun' defines the output parameter 'val'. 'val' examines the overlap between the white area in the data image (BW4) and the image of the drawn circle (crcl), as well as the overlap of the white area in crcl and the black area in BW4. The value of a drawn circle is finally determined by

$$\left[val = | \frac{1}{\Big(||BW \cup crcl|| - ||crcl \cup \tilde{BW}|| \Big)} \right] | \tag{2.25}$$

Where $||BW \cup crcl||$ and $||crcl \cup \tilde{BW}||$ are the sizes of the overlaps.

Chapter 3

Results

The purpose of the results section is to record and organize the contact angle data obtained from experimentation. All deviations from procedure discussed in the Methods section are recorded in this section.

The temperature-dependence of water's contact angle has been measured for three different substrates: graphite, silicon, and gold. Graphite and gold were chosen for study because contact angles of water on these surfaces has already been studied, thus creating a reference point. Silicon was chosen for study, because water on silicon has a low contact angle at room temperature. This is important because according to the theory discussed in the introduction, a smaller contact angles will experience a wetting transition at lower temperature, thus making them easier to observe.

The temperature was increased from room temperature to the max temperature of the experiment over a period of between 4 and 8 hours. This rate of temperature increase was chosen because slower rates caused droplets to form on cell windows, thus obstructing contact angle observation. At higher temperature rates of change, the heat gradient between the cell windows and the substrate water causes condensation on the substrate.

The sharp-kink approximation tells us how the droplet's contact angle should change with temperature. When the experiment begins at room temperature, the contact angle will have an initial value, θ_0. The sharp-kink approximation tells us that as temperature increases, the contact angle should continuously and monotonically decrease, until a critical temperature T_w. At this critical temperature the droplet stops decreasing monotonically, and instead undergoes a wetting transition. The wetting transition causes θ to immediately become $\theta = 0^\circ$. The contact angle then remains zero for all temperatures greater than T_w.

In the majority of experiments that took place to find the critical temperature of water on graphite, silicon, and gold, a wetting transition was not observed. In fact, only one wetting transition was observed, although there were signs that a second wetting transition had occurred. Furthermore, the observed contact angles did not always decrease monotonically. Throughout experiments,

the contact angle changed in several different ways, including: increasing on the average, remaining at constant contact angle, decreasing monotonically, and initial decrease followed by a dramatic increase in contact angle.

Therefore, if according to the sharp-kink approximation, the only expected result is a monotonic decrease in contact angle as temperature is increased then the assumptions about the water, the substrate, or the atmosphere were incorrect. To determine the cause of the deviation from theoretically predicted contact angle, we studied the following possible reasons that could explain why the contact angle behaved in a non-homogeneous manner throughout experimentation: impurity of water, evaporation, inhomogeneity of temperature, and differing saturation conditions, temperature gradients.

3.1 H_2O on Graphite

This section reports the measured changes of contact angle of water on ZYA graphite as a function of temperature. During experimentation, temperatures ranged between 25 and 130 °C, although only one experiment reached this high temperature, while the rest had a maximum temperature below 80°C. Water was used from three different sources to determine whether water purity affected contact angle. Further testing was done on droplets that had been positively charged to test charging effects.

The tables that include original measurements of the contact angle are in Appendix I. The same piece of graphite was used in all of these experiments, but in order to use an unadulterated surface in each experiment, a clean layer of graphite was revealed immediately before beginning each new experiment. If the process of removing a few layers of graphite did not significantly change the graphite, then the variation in initial contact angle was not due to difference in substrate material, and that the could only be caused by variations in water and atmosphere. The initial contact angle that water made with the graphite substrate varied from below 85 degrees to more than 114 degrees.

3.1.1 Stored Water

In this early experiment, the water that was used came from a container that had been stored in the lab, and had been de-ionized to 17.5 MΩ-cm several months previously. The water had not been tampered with in this container, but it was not newly filtered. In this experiment, the cell was left in the silicone bath overnight to equilibrate before experimentation. In later experiments, it was found that teflon O-rings used to seal the cell became contaminated with the silicone oil used in the bath when the cell was left in the bath overnight. This casts doubt on this and other early experiments.

Figure 3.1 shows the change in contact angle of a $2.0 \pm 0.2\mu$L droplet of H_2O on graphite. The water used during this experiment was not filtered for high purity, but was de-ionized several months before the experiment took place.

$400 \pm 40\mu$L reservoir of water was used to help prevent droplet evaporation. Water was not placed directly under the reservoir in this early experiment.

It was found that between 26.5 and 87.7°C the contact angle did not change. At temperatures above 100 °C the contact angle starts increasing. One possibility that might explain why the contact angle was increasing could be that the droplet was evaporating. By using the program to measure the relative size of the droplet, the droplet volume could be monitored. it was measured that while the contact angle was increasing, the droplet was becoming smaller.

In Figure 3.1 the black squares show the contact angle, measured in degrees. Temperature is measured in °C. The temperature of the cell was measured every 30 seconds throughout the experiment, thus the cell's temperature was known within an precision of less than 0.05 °C. Corresponding error bars would not show up on the graph.

The open circles in Figure 3.1 show the measured fractional change in volume of the water droplet. Each open circle shows the relative droplet volume with respect to the first droplet of the picture. This picture shows that at 87.7°C the droplet has decreased in volume by 46.7±1.5% when compared with the volume at 26.5°C.

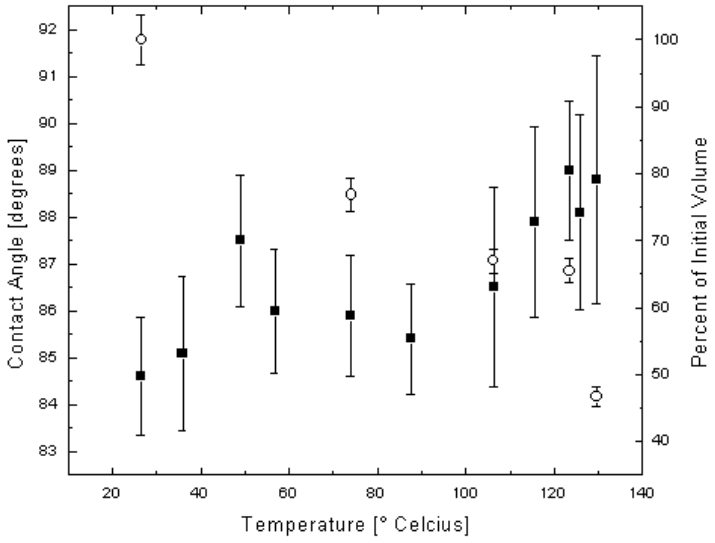

Figure 3.1: Results of the Contact Angle vs Temperature measurements of stored water on graphite, described in detail in section 3.1.1. Contact angles are represented by black squares and were obtained by averaging the contact angle of several values that came from the Matlab program discussed in section 2.3 written in this experiment. The error bars were obtained by taking the standard deviation of the same values. Measurements of relative volume are represented by open circles. Each open circle data point shows the relative droplet size with respect to the volume of the first droplet in the experiment. More information on data analysis methodology can be found in the methods section.

3.1.2 New Water

In the experiment above, although water was placed in the cell with the droplet as described in the *Methods* section no special care was taken to make sure the reservoir of water within the cell was directly under the graphite sample during the first experiment. Thus experimenters theorized that the reservoir did not completely saturate the air around the droplet with water vapor, and saturation conditions were not met, in turn inducing droplet evaporation.

To test if water resistivity changed the results, water that was filtered to a purity of 18.2 MΩ-cm the day of experimentation was used. This is different than the previous experiment in that this experiment did not let the droplet sit in the silicone oil bath for any significant amount of time before experimentation. This experiment used a $600 \pm 10\mu$L reservoir of water, which was placed directly under the reservoir to deter evaporation.

One of the difficulties in the analysis was that the photographs taken during this experiment had noise that caused the Matlab program to incorrectly select the dark region of photograph to be processed as part of the droplet. In order to calculate a contact angle, the photos were altered to remove these darker regions. This is shown in Figure 3.2

The reason that the error bars on this experiment are so high is that the Matlab program had a hard time determining an appropriate circle that would fit the droplet. The background in these pictures had artifacts that distorted the Matlab program's perception of droplet shape. This distortion made contact angle analysis impossible, and thus was edited away. Removing the came at the cost of not having Matlab be the only judge of droplet boundaries. Images altered by humans do not preserve the circularity of droplets, and thus determining an appropriate circle that would fit the droplet lead to greater error. Figure 3.2 shows the difference in altered and unaltered images.

Unlike Figure 3.1 experiment of water on graphite, the results of this experiment, showed the contact angle decreased with temperature at the beginning of the experiment, and then increased later. The contact angle dropped from 85.9 ± 1.7 to 78 ± 2 degrees as temperature increased from 24.9 to 43.9°C. By 56°C the droplet had begun to decrease in size. Between 44 and 56°C there was a spike in both contact angle and droplet size. The sudden change in droplet size was not due to any camera adjustments, and therefore must have been due to reduction in droplet volume. By the end of the experiment, the droplet has decreased to 77±4% of its initial size, and simultaneously experienced an increase in contact angle to 97±3°C.

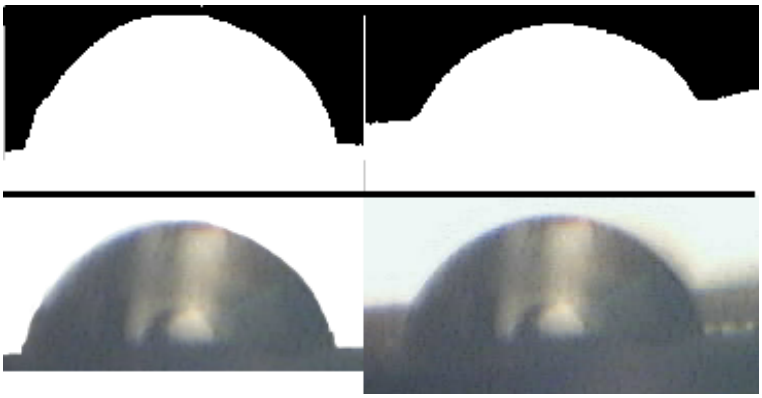

Figure 3.2: An unaltered image and the Matlab interpretation of that unaltered image are shown on the top, while an altered image and its interpretation are shown on the bottom. The unaltered image's Matlab interpretation clearly does not measuring the contact angle that corresponds to the unaltered image. The altered image compromises the systematic nature of using the Matlab program, but does give a range of plausible contact angles.

3.1.3 Two Increased Droplet Size Experiments

Two experiments were conducted to test if increased droplet size was a major factor during experimentation. In all other regards these two experiments are like the previous experiments except that they used a $1.5 \pm 0.1\mu$L droplet rather than a 1.0μL droplet.

In the first of the two experiments with increased droplet size, Figure 3.4 shows the droplet had an initial contact angle of about 98 degrees. Throughout the entire experiment, between 28.5 and 76.0 °C, there is no change in contact angle within experimental error. Above 76 ° C, the contact angle remained approximately constant at 98 ± 3 degrees.

A second experiment took place with the same initial conditions because results from the first experiment were unexpected and different from the theory.

During the second experiment, a crack appeared in the glass window around the time when the last picture was being taken. Further inspection showed that no oil seemed to enter the cell, and the sample did not seem to be contaminated, but the leak necessitated immediate care, and thus experimentation to higher temperatures was not pursued.

Before this point, Figure 3.5 shows the highest initial contact angle (contact angle at room temperature) recorded for water on graphite: 115 degrees. That contact angle monotonically decreased over the entire temperature range of the experiment until 64.9 °C, when the contact angle was 103 degrees and the experiment needed to be stopped for reasons mentioned above.

Overall, the contact angle decreased from 114.7 ± 1.8 to 102.6 ± 1.6 degrees,

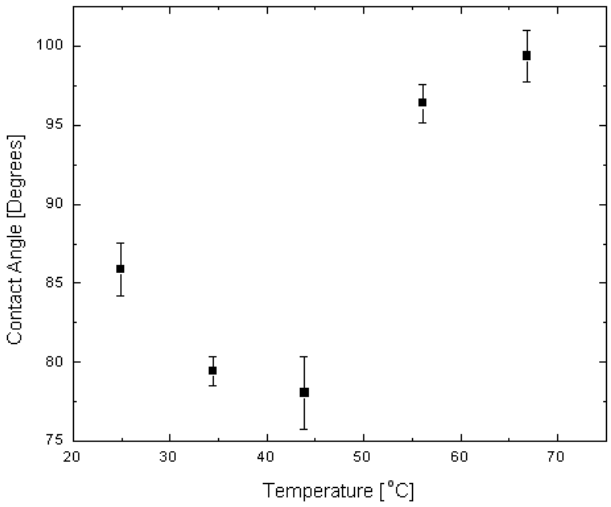

Figure 3.3: This experiment of water on graphite used water that had been purified that day. This also differed from the previous experiment in that the reservoir of water in the cell was placed directly under the droplet instead of in the arm of the cell. During this experiment the contact angle (black squares) decreased between room temperature and 44 degrees and then had increased to above 90 degrees by 55 ° C. One possible reason for the spike in contact angle is droplet evaporation.

with most of the decrease in contact angle happening in the later parts of the experiment. Between 51.5 and 64.9 °C and the end of the experiment (just more than 13 of the temperature range of the experiment), the contact angle dropped 65.6 degrees (just less than 23 of the entire change in contact angle of the entire experiment).

These two experiments that took place with a droplet that was 1.5μL did not share similar behavior. The contact angle from the first experiment remained 98 over the temperature range of the entire experiment, while the second contact angle behaved like many of the 1μL droplets observed during experimentation, and had a monotonically decreasing contact angle. One similarity between the two droplets is that both had a large initial contact angle when compared to 1 μL droplets at equal temperature.

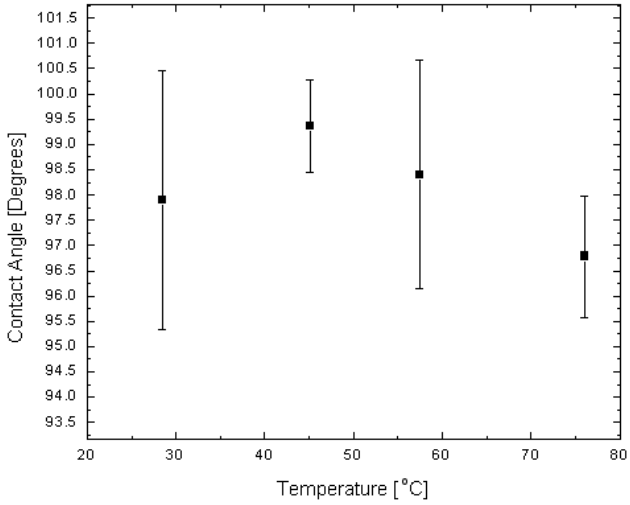

Figure 3.4: Change in contact angle vs temperature with a slightly larger droplet size of 1.5μL, the first of two experiments studying effect of droplet size on contact angle. Large error bars are due to image altering techniques, this issue is further discussed in the Methods section. This experiment produced curious results in that the contact angle remained constant throughout the experiment. A follow-up experiment with the same initial conditions was run, to check the consistency of this experiment.

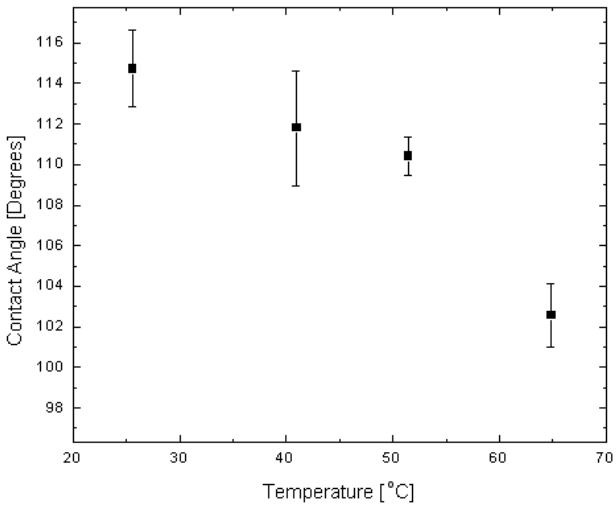

Figure 3.5: Change in contact angle vs temperature with a slightly larger droplet size of 1.5μL, the second of two experiments studying effect of droplet size on contact angle. This experiment had monotonically decreasing contact angles over the full temperature range of the experiment, but was cut short because the cell started leaking.

3.1.4 Charged Droplets

The wide range of initial contact angles were seen, with water from different sources, suggests that there might be some charging effects that could have instigated the wide range of initial contact angles seen during experimentation.

To test this, two droplets were charged and allowed to equilibrate before having their contact angle examined. Figure 3.6 shows a typical initial contact angle of a charged droplet of water. The initial contact angle of these droplets was found to be 95.4 ± 1.0 degrees.

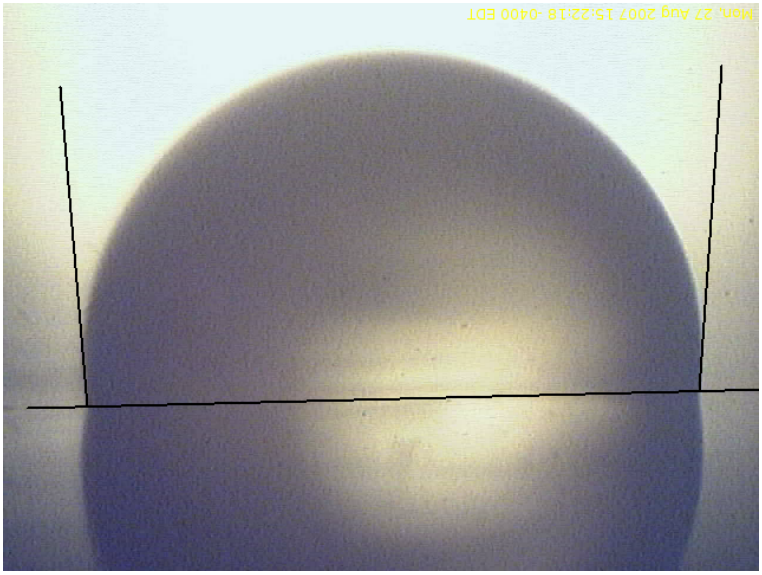

Figure 3.6: A typical initial contact angle of a charged droplet of water. This image is indicative of all the initial contact angles of droplets charged water on graphite. The contact angle of this droplet at room temperature is 95.7 ± 0.7 degrees.

3.2 H_2O on Silicon

This section reports the measured changes of contact angle of water on silicon (100) as the temperature is increased from 25 $\pm 3\,^{\circ}$C to $80 \pm 3\,^{\circ}$C. We used the experimental set-up described in the methods section. The tables that include original measurements of the contact angle are in Appendix I.

Throughout experiments, the contact angle responded to an increase in temperature in several different ways. In response to an increase in temperature, it was experimentally found that the contact angle was in one instance increasing. There were three experiments where the contact angle of water on silicon did not change appreciably throughout the experiment. In the remaining four experiments the contact angle was decreasing. Whether or not a contact angle decreased or stayed the same did not seem to be due to differences in substrate preparation. Furthermore, during two experiments of water on silicon there was evidence that a wetting transition occurred, although the phenomenon was only observed once, and it was never documented photographically.

Many of the photographs taken during experiments of H_2O on silicon had noise that caused the Matlab program to incorrectly select the dark region of photograph to be processed as part of the droplet. In order to calculate a contact angle, most photos were altered to remove these darker regions. Those photos not altered have been noted in the text below.

The tables that include original measurements of the contact angle are in Appendix I.

3.2.1 Stored Water

This section describes two experiments with nearly the same preparation. In these experiment, the water that was used for both the droplet and the reservoir came from a container that had been de-ionized to a resistivity of 17.5 MΩ-cm several months previously. The water had not been tampered with in this container, but it was not newly filtered. It was used because it was water that was on hand, furthermore it had already provided water for the experiment described in Section 3.1.1. The cell was set in silicone oil overnight before experimentation started, and it is possible that the cell was contaminated during that time

Data from the first of two experiments is reported in Figure 3.7. The figure shows the measured change in contact angle of a droplet in a cell with a $400 \pm 30\mu$L reservoir of water. Water was not placed directly under the substrate in this early experiment. It was noted in this experiment that there was a temperature gradient within the cell near the windows. The temperature gradient appears within the cell because the cell is not at the same temperature as oil surrounding it for the duration of the experiment. In this experiment, the substrate was near to one window of the cell, which, in the presence of the temperature gradient, caused evaporated water droplets to condense on the silicon substrate. These condensed droplets obstructed droplet visibility, and thus experimentation was stopped above 60 °C.

Figure 3.7 shows the contact angle continually increasing from 38.0 ±0.8 to 46.3±1.0 degrees between the temperatures of 33.4 and 59.6 °C. The experiment was stopped early due to substrate being covered with condensing droplets. Droplet size was observed to decrease linearly to 62±3% of the initial volume. In most experiments the droplet maintained more than 75 % of its original volume. It could be that during this experiment the air was becoming less humid due to water condensing onto the substrate, and thus more water evaporated from the droplet in response to the incomplete air saturation within the cell.

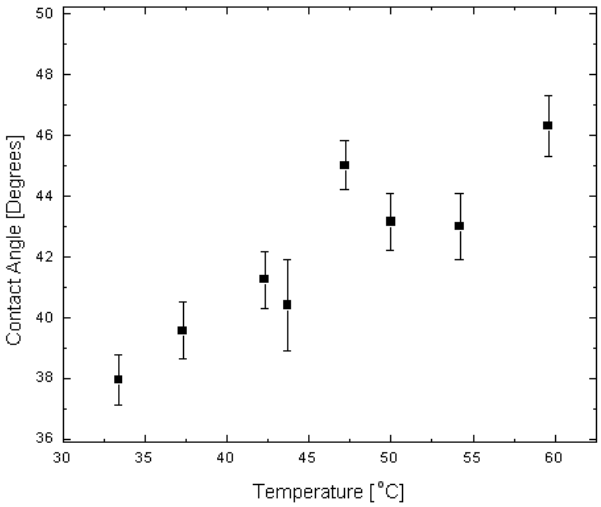

Figure 3.7: Results of the Contact Angle vs Temperature measurements of stored water on silicon, described in detail in Section 3.2.1. Contact angles are represented by black squares and measurements of relative volume are represented by open circles. Each open circle data point shows the relative droplet size with respect to the volume of the first droplet in the experiment.

The second experiment was performed with the same initial conditions described earlier in this section, with the exception that in the second experiment the cell was grounded directly before experimentation in order to mitigate charging effects. Further detail about why we grounded the cell can be found in Section 2.1.2.

The results of the second experiment show the contact angle was found to not change between 25 and 75 °C, which is to say, the entire range of the experiment.

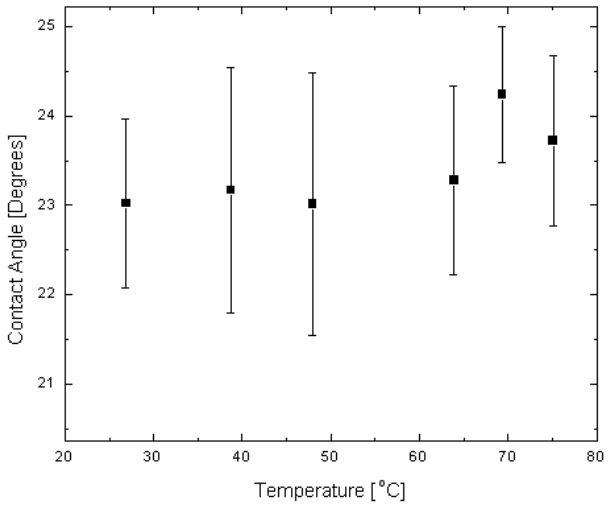

Figure 3.8: Contact angles of a droplet of stored water in a grounded cell. The average is slightly shifting about 23 degrees, but within the error bars of the experiment, there is no significant increasing or decreasing trend.

3.2.2 New 17.5 MΩ-cm Water

This experiment is different from the latter two in that in this experiment 400 μL of water was placed directly under the silicon substrate, a procedure that would be used during the rest of experimentation. Also the cell did not sit in the silicone oil overnight, because it was suspected that increased exposure to the oil increased possibility of cell contamination. Although the water was new, it was only filtered to 17.5 MΩ-cm because this was the first time we suspected water purity might be affecting contact angle behavior. Later we would use water that we filtered with new equipment to 18.2 MΩ-cm.

Figure 3.9 shows that in this experiment the data started decreasing like in several other experiments. Contact angle decreased from 31 to 26 degrees between the temperatures of 30 and 45°C. After the final picture was taken, an experimenter observed the droplet spread out and slide to the left (the cell was tilted slightly so that left was slightly lower than the right). Some time passed after the cell had been righted to this new, more stable position, when seemingly all of a sudden, the droplet trickled off the silicon substrate.

This was believed to be a wetting transition at the time, but whether or not this is the case is uncertain. Noteworthy is that nothing bumped or jarred the apparatus in any way, and the droplet seemed to move spontaneously.

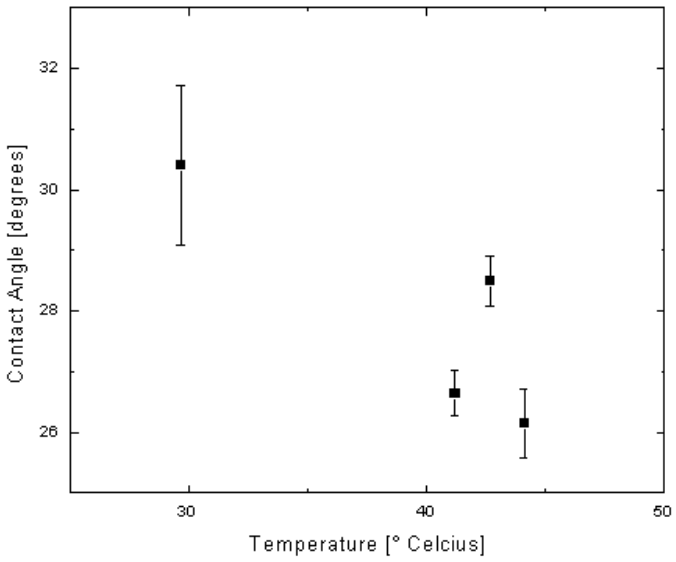

Figure 3.9: Contact angle vs temperature of a droplet of freshly de-ionized droplet with resistivity 17.5 MΩ-cm water. During this experiment, observers saw a wetting transition at 44.5°C. Just before the droplet disappeared, the contact angle was measured to be 26 degrees.

3.2.3 Standard Procedure

This section reports on an experiment in which all methods of cell, substrate, droplet, and reservoir preparation were exactly as reported in the Methods section, with no deviation. This is different from the previous experiments on silicon in that the water was de-ionized to a resistivity of 18.2 MΩ-cm. It is supposed that higher resistivity water has a higher proportion of H_2O and less impurities.

Figure 3.11 show the contact angle decreased on the interval between 24 and 45 °C. Figure 3.10 show that at 45 °C the droplet disappeared from pictures, leaving behind a thin, shiny surface of water on the silicon. This phenomenon was believed to be a wetting transition. This second occurrence of the wetting transition was the last time such a behavior was observed.

Figure **??** shows two consecutive pictures from this experiment. In the first, the full 1 μL droplet is on the silicon, and in the center of the camera. In the second, there is a little bit of water residue visible at the edge of the picture, but the majority of the water is missing. An experimenter did not view the wetting transition, but if this experiment was similar to the previous experiment, the water suddenly started moving and flowed until it reached the edge of the silicon or the edge of the cell. Water at the edge of the silicon may have been stopped from rolling off of the substrate by pinning forces.

3.2.4 Stored Water- Revisited

This experiment tested whether or not leaving the cell in the silicon bath overnight had an effect on the contact angle. The only experiments that had the cell left in the silicon bath over night were the first two experiments, those using water stored in the lab that had been filtered to a resistivity of 17.5 MΩ-cm several months previously. Thus in testing whether or not overnight storage in silicone oil made a difference, the same stored water was used to minimize discrepancies between experimental methods.

Figure 3.12 shows that the droplet's contact angle remained relatively constant between the temperatures of 24 and 38 °C. But by 41 °C the contact angle had dropped 5 degrees to about 25 degrees. The contact angle remained at this low point until the end of the experiment.

This behavior is inconsistent with the two experiments where the oil was allowed to rest in the cell overnight. Furthermore the theory predicts results that are much more similar to the results obtained in this experiment. Because this was the case, in all subsequent measurements the cell was not stored in the silicone oil bath before experimentation, and the behavior of the other experiments with the lab's stored water were considered contaminated.

Noticing that contamination was the potential cause of a whole host of differing results, only water with resistivity of 18.2 MΩ-cm that had been purified that day was used in future experiments.

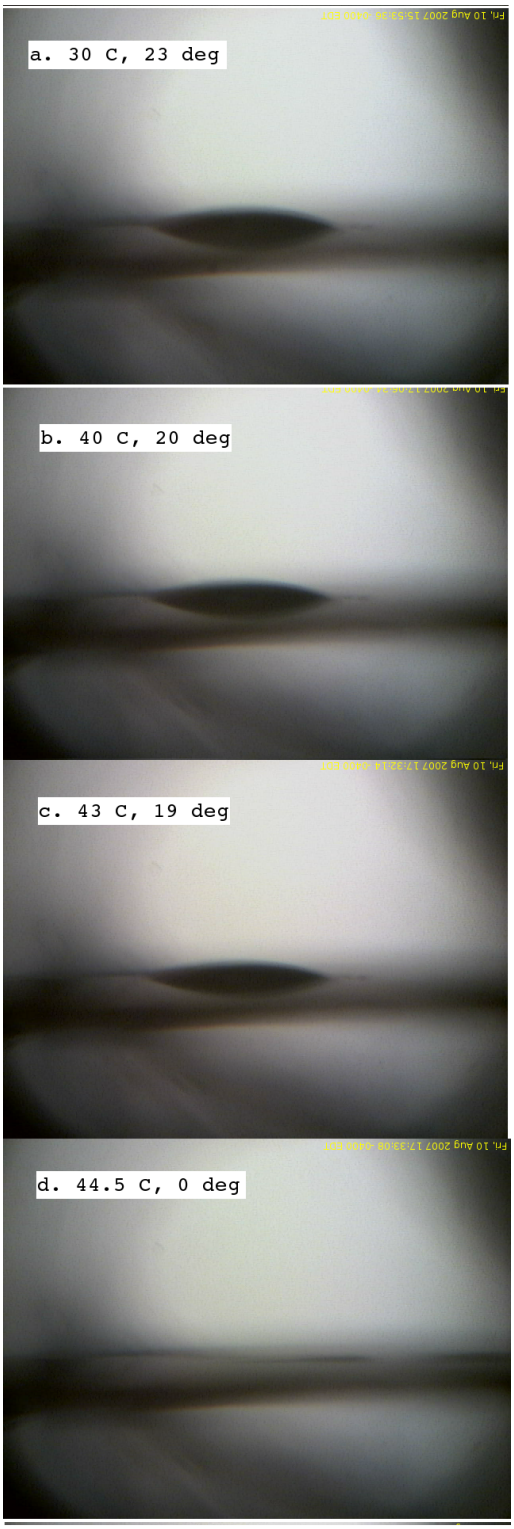

Figure 3.10: This set of four pictures shows a wetting transition. The pictures (a,b,c,d) of the experiment had the following had (Temperature, Contact Angle) given below. Because the droplet disappeared so suddenly experimenters believe the droplet to have undergone a wetting transition.

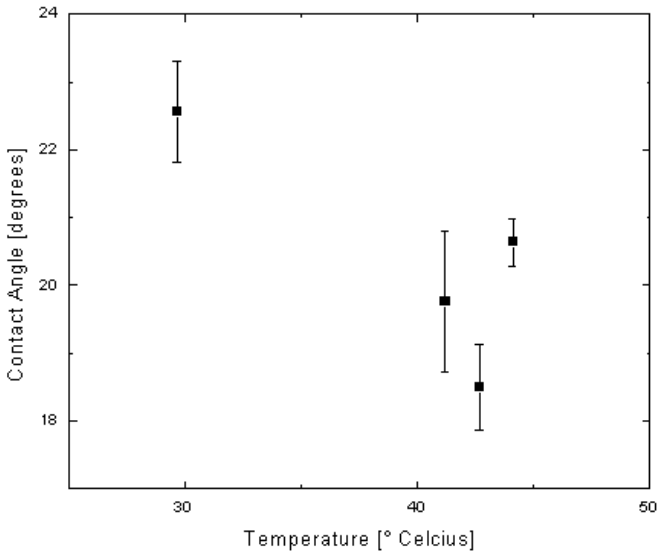

Figure 3.11: Contact angle vs temperature results when we followed the exact procedure outlined in the Methods section. This experiment used 1 μL of 18.2 MΩ-cm water on silicon. During the experiment, the droplet disappeared from view. It is possible this could be due to the droplet undergoing a wetting transition. Before the droplet disappeared, the final measured contact angle was 19.5$\pm$1.5 degrees.

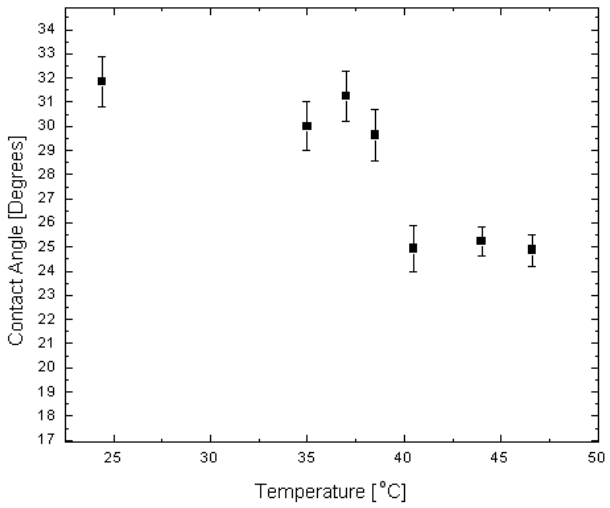

Figure 3.12: Results of the Contact Angle vs Temperature measurements of stored water on silicon. At first the contact angle is unchanging within experimental error, but does decrease on the average from 32 to 30 degrees. At about 40 °C the droplet then experienced a large drop in contact angle to about 25 degrees.

3.2.5 Grounding the Cell

Because the previous experiment showed that the experiment where the cell had been grounded was potentially invalid, two follow-up experiments were done using 18.2 MΩ-cm water that had been de-ionized that day. The two experiments were almost identical in preparation, the difference between the two being that the first experiment had a 400 μL water reservoir, and the second had a 600 μL reservoir. The larger reservoir was added because the droplet began to evaporate in the first experiment.

The first experiment's results are shown as the open triangles in Figure 3.13. The experiment only spanned 33 to 53 °C, but on this range the contact angle monotonically dropped from 23.5 to 14.2 degrees. The experiment was stopped when the droplet began noticeably changing in volume. The second experiment's results are conveyed as the black squares in the same Figure 3.13. The contact angles were measured between 22.8 and 70.2 °C and on this range the contact angle dropped from 22.6 to 18.8 °C. Although a larger reservoir of water was added to the cell the droplet still appeared to be evaporating.

The two experiments shared very similar results: both monotonically decreasing, had droplets that were evaporating, and neither yielded a wetting transition.

Furthermore it was realized that the ground that was used might not be completely neutral. If the ground was not neutral the 'grounding' done in the preparation procedure might have charged the cell. Additionally, it is possible that the cell was charged after being grounded and before being placed into the bath, because it is impossible to say with certainty that the devices used to manuver the cell into the silicone bath were not charged.

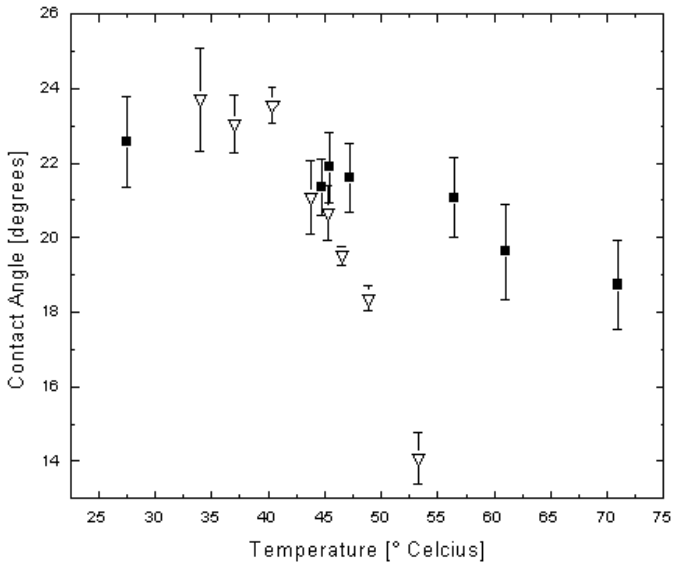

Figure 3.13: Two experiments with a droplet de-ionized to 18.2 MΩ-cm and with a cell that was grounded. The two exhibit similar behavior but have a different initial contact angle. Experimentation was stopped in both cases because the droplet was noticeably evaporating. The two initial contact angles were both approximately 23 degrees, but in the first experiment the contact angle dropped to 14 degrees, whereas in the second it only fell to about 19 degrees.

3.2.6 Saltwater

To neutralize any charges within the droplet, sodium chloride was added to the water before experimentation began. By neutralizing the charges in the droplet, we tested how an uncharged droplet behaved differently from a possibly charged droplet.

This experiment used a combination of water de-ionized to 18.2 MΩ-cm and NaCl, unlike previous experiments that used just de-ionized water. The saltwater solution was a mixture of 60.0±0.1 g H_2O with 1.00±0.05 g NaCl. 2 μL of saltwater was placed on silicon (100) during the preparation of this experiment.

The initial contact angle of saltwater on silicon was 33.9 degrees. As the temperature increased to 70 °C, the contact angle dropped to 26.8 degrees. Beyond 70 °C, the contact angle remained approximately constant. It is noteworthy that the final contact angle of this experiment of saltwater on silicon was greater than the observed initial contact angle of H_2O on silicon for more than half of the experiments conducted, and the final value from Figure 3.14 is approximately the same as the 25 degree is the contact angle observed at the beginning of most experiment.

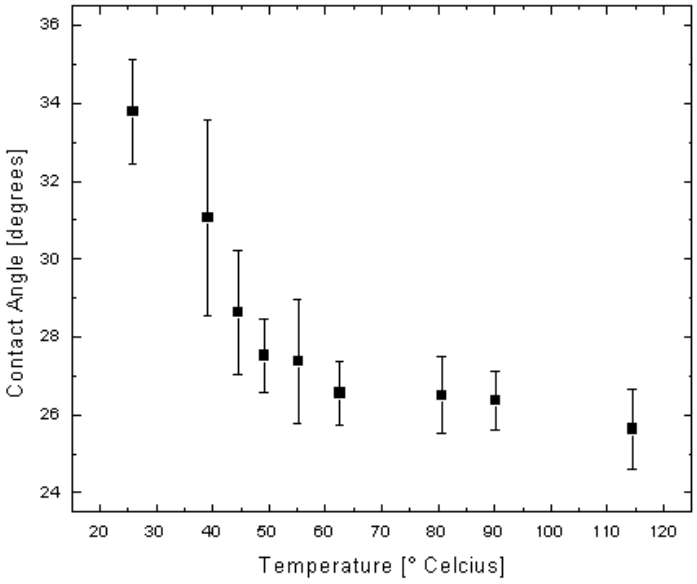

Figure 3.14: Although the initial contact angles were vastly different, the behavior of saltwater on silicon below 70 °C was similar to experiments where the cell was discharged. On this range, the contact angle decreased significantly in both cases. The fact that the contact angle does not increase above 70 suggests that the droplet was pinned at this value.

3.2.7 Charged Droplet

To further study the effects of charging on contact angle, we tried to intentionally charge a droplet and observe the change in contact angle vs temperature under the new conditions. The droplet was composed of water de-ionized to 18.2 MΩ-cm. After the droplet was secured on the silicon, an aluminum sheet, on which the prepared silicon rested, was bombarded with positive charges from an air purifier. This presumably would leave the silicon and substrate positively charged. More information about preparing the charged cell can be found in the Methods section.

Figure 3.15 shows the behavior of temperature on contact angle between 20 and 85 °C. The initial contact angle was 30 degrees. Between the temperatures of 40 and 65 °C, the contact angle increased to 32 degrees. Above 65 °C, the contact angle plummeted to 22 degrees, which is where the experiment stopped due to droplet evaporation.

This behavior is not similar to experiments where the cell was left uncharged. Because the behavior is drastically different, it is plausible that charging effects contact angle.

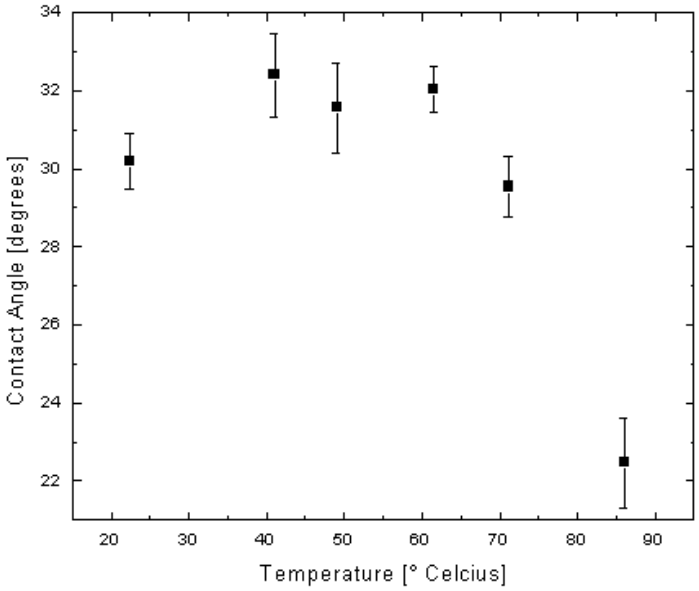

Figure 3.15: The change in contact angle vs temperature of a charged droplet of water. Notice the high initial contact angle, and the increase in contact angle before falling to 22 degrees.

3.2.8 Larger Droplet

This experiment uses a 1.5 μL droplet of water de-ionized to 18.2 MΩ-cm. It is different from the other experiments in this section in that its purpose was to examine the how the initial droplet volume effects the contact angle vs temperature-dependence for water on silicon. This experiment only deviates from the standard procedure in that the droplet volume used was 1.5 μL instead of 1.0 μL.

Figure 3.16 shows the variation in contact angle with increasing temperature. The experiment starts off with an initial contact angle of 26 degrees, which is on the slightly high end of initial contact angles for purified water. The contact angle remains approximately constant between room temperature and the time when the experiment stops at 80 °C.

This behavior was unexpected and is not in line with observations made on droplets of slightly smaller size. This experiment seems to demonstrate that there are variables in this experiment that are not being controlled. Furthermore it seems that these variables can dramatically change the results of the experiment.

Figure 3.16 shows that the contact angle did not change within the error of the experiment between the temperatures of 20 and 80 °C. Throughout the experiment the contact angle was approximately 23 degrees. Experimentation was stopped because the contact angle could no longer be extrapolated from the picture.

3.3 Water on Gold

This experiment used standard droplet and reservoir size and placement within the cell. In this experiment we used 18.2 MΩ-cm water for the droplet and reservoir. The droplet was placed on the gold surface, following the procedure described in the Methods section. For water on gold, the shark-kink approximation predicts a monotonically decreasing contact angle as temperature is increased.

As can be seen in Figure 3.17 the initial contact angle is 56 degrees at 25.2 °C, and then grows with temperature for the duration of the experiment. At the end of the experiment, the contact angle is 73.6 degrees while the temperature is 101.3 °C. Experimentation was stopped because the temperature controller cut out, as described in the Methods section, and thus higher temperatures could not be obtained.

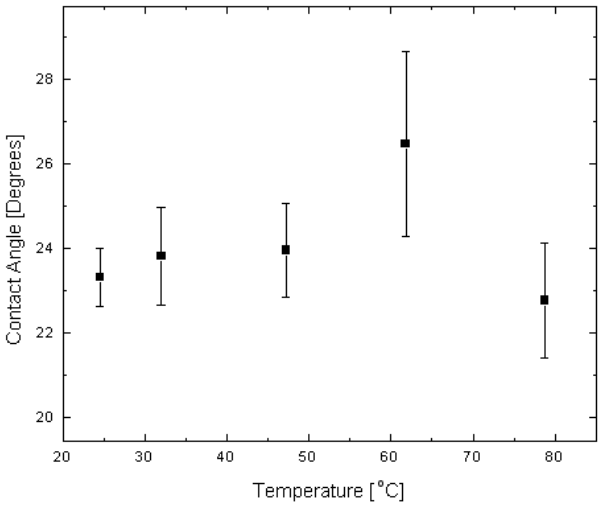

Figure 3.16: Contact angle vs Temperature measurements of a 1.5μL droplet of water on silicon. The constant contact angle is an unexpected result.

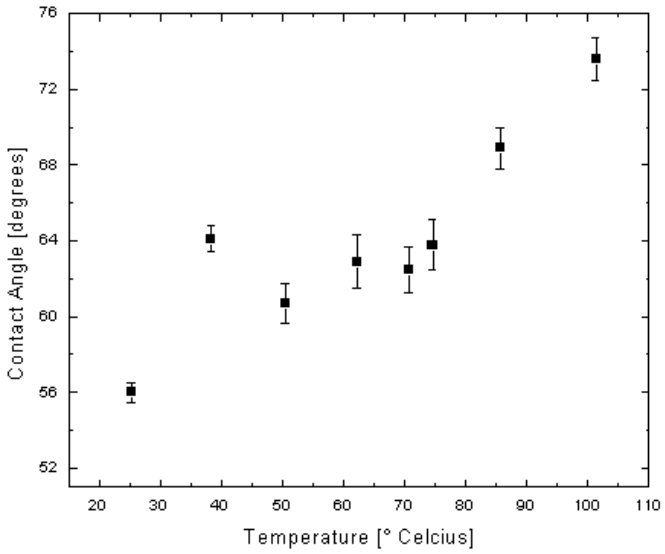

Figure 3.17: Contact angle vs Temperature measurements of a 1.5μL droplet of water on gold. The shark-kink approximation predicts a monotonically decreasing contact angle as temperature is increased, while this figure shows contact angle growing as temperature is increased.

Chapter 4

Discussion

The contact angle of water on graphite silicon and gold was measured between the temperature of 20 and 150 °C. As temperature increased, the contact angles was observed to behave in several different ways, including increasing, decreasing, and not changing.

4.1 Theory vs Experiment

We measured the contact angle of water on graphite, silicon, and gold as temperature was increased.

For the contact angle vs temperature-dependence for water on graphite, silicon, and gold is given by the following relation in the sharp-kink approximation, Eq. 4.1. We sought to examine whether this approximation, using only van der Waals type forces, successfully predicted the contact angle's temperature-dependence. According to Eq. 4.1 the contact angle is expected to decrease monotonically until the wetting temperature, T_w, is reached. At T_w and all higher temperatures the contact angle is expected to be zero degrees.

$$\cos\ \theta = -1 + \frac{\Delta\rho}{\sigma_{lg}}(T)\, I \tag{4.1}$$

Here $\Delta\rho$ is the difference between liquid and vapor densities, σ_{lg} is the liquid gas surface tension, T is the temperature, θ is the contact angle, and I is the van der Waals integral. In our case the liquid is water, and the surrounding vapor is air. Here the parentheses indicate that σ_{lg} and $\Delta\rho$ are functions of temperature.

I is dependent on the type of liquid molecule and the substrate. In our calculations using Eq. 4.1 we assumed that I was temperature independent and moreover was constant. I was calculated by integrating van der Waals attraction and repulsion energies of the particular liquid and substrate with van der Waals coefficient C and well depth D. Alternately, by assuming Eq. 4.1 to hold, we calculated I from experimental observations using

$$I = \frac{\sigma_{lg}}{\Delta\rho}(T)\,[1 + cos\theta] \tag{4.2}$$

These different methods for determining I predict different contact angles, and both methods were used to analyze the data.

4.1.1 Water on Graphite

We investigated water on graphite because others papers [] [] [] had measured the contact angle at room temperature for water on graphite. We measured the contact angle of water on graphite while increasing temperature from 20 to 130 °C. The maximum temperature reached during experimentation was 130 °C, and no wetting transition was seen. Initial contact angles varied widely over the four experiments of water on graphite, and are listed in Table 4.1. The main result was that contact angle behaviors varied widely between experiments.

Table 4.1: List of Initial Contact Angles of Water on Graphite

Experiment Name, Section #	Room Temp [°C]	Contact Angle [degrees]
Stored Water , 3.1.1	26.5	84.6
New Water, 3.1.2	24.9	85.9
Increased Droplet Size (1), 3.1.3	28.5	97.9
Increased Droplet Size (2), 3.1.3	25.6	114.7
Average	26.4	95.8
Eq. 4.1	26.6	88.1

The observed contact angles do not accord with the data. Plugging in average temperature and contact angle, $T = 26.38°\text{C}, \theta = 95.78°$ yields

$$I = 64.4 \pm 10.1\ \mu\text{J m kg}^{-1} \tag{4.3}$$

For comparison, the van der Waals integral calculated C and D is

$$I = 71.47 \pm 0.07\ \mu\text{J m kg}^{-1} \tag{4.4}$$

Figure 4.1 displays the contact angle vs temperature-dependence for water on graphite along with predicted contact angles. The predicted contact angle of water on graphite using $C = 12500 \pm 200$ KÅ^3 and $D = 1170 \pm 120$ K [31] to determine I is displayed as an an unbroken curve, while the unbroken line displays I by using the average temperature and angle from Table 4.1 and Eq. 4.2. The four experiments showed four different behaviors for the temperature-dependence of the contact angle of water on graphite. The experiment using Stored Water showed that contact angle increased with temperature.

Another result was that in the experiment using New Water, the contact angle initially decreased, but later increased. The first experiment using increased

droplet size showed contact angle did not change with temperature, and the second experiment using increased droplet size showed that contact angle decreased with temperature.

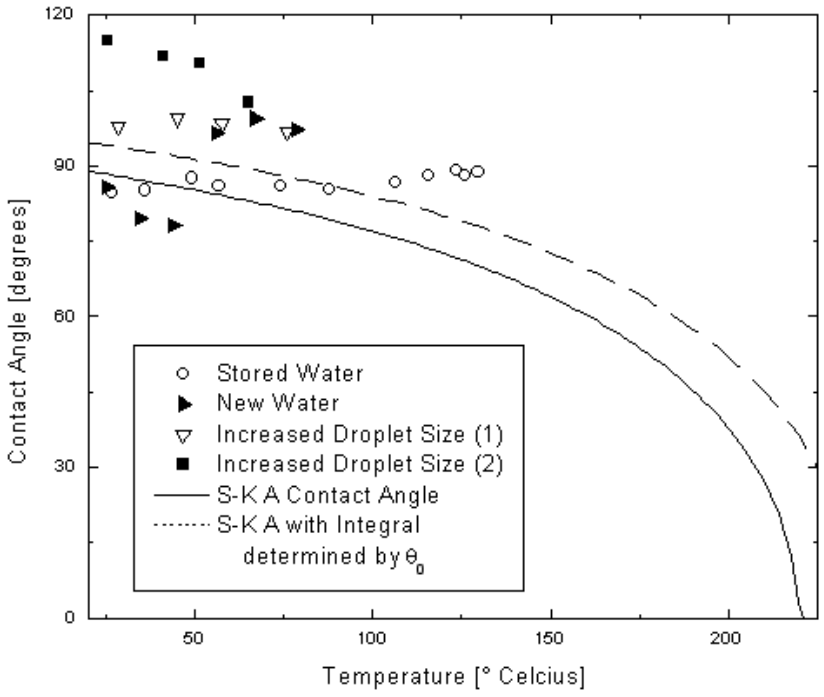

Figure 4.1: The results from the four experiments of water on graphite, each of which is labeled in the legend. The unbroken curve is generated from Eq. 4.1 and use of van der Waals coefficients C and D[31], while the broken curve is generated from the sharp-kink approximation and use of initial contact angle at room temperature, to experimentally determine a value for the van der Waals integral I.

Initially it might be unsettling that deviation from theory is greater in higher end of the experimental temperature range, but the data in question was from the Stored Water experiment of water on graphite. Possible reasons for this are discussed later in the Experimental Deviation and Sources of Error sections.

4.1.2 Water on Silicon

We investigated water on silicon because water has a small contact angle on silicon and therefore, according to Eq. 4.1, we would expect a much lower T_w. Experiments took place between 20 and 120 °C, and saw evidence of two possible wetting transitions. However results varied widely from experiment to

experiment.

Temperature-Dependence of the Contact Angle

Figure 4.2 shows that the contact angle of water on silicon decreased monotonically in seven out of the ten experiments. This was even true independent of when the cell was charged, or grounded, or if the liquid used was saltwater. The rate of monotonic decay varied throughout the seven decreasing experiments, In the first experiment where we grounded the cell the contact angle decreased 10 degrees over a 20 °C change in temperature, while in a very similar experiment where we grounded the cell, the contact angle changed by 3 degrees over 40 °C change in temperature.

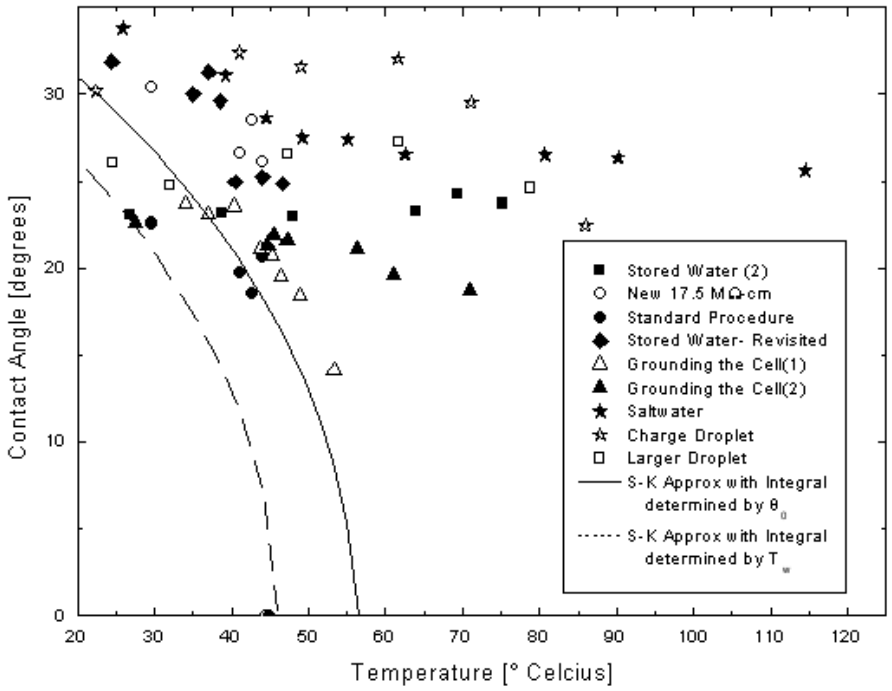

Figure 4.2: The results from the ten experiments of water on silicon, each of which is labeled in the legend. The theory curve is generated from the sharp-kink approximation and use of initial contact angle at room temperature, to experimentally determine a value for the van der Waals integral I. Results from experiment Stored Water(1) are not shown for reasons of visibility.

Of the three experiments that did not decrease monotonically, Stored Water (2) and Larger Droplet did not change in contact angle, while Stored Water (1) increased in contact angle. As with graphite, the experiments using the water

the had been de-ionized to a resistivity of 17.5MΩ-cm several months previously.

Initial Contact Angle determined I

The initial contact angles varied from 22.4 to 34.0 degrees at room temperature. A complete list of contact angles is given in Table 4.2. Using the average initial contact angle and temperature from the water on silicon experiment, it is possible to determine the van der Waals integral using Eq. 4.2. The average temperature and contact angle from Table 4.2, $T = 28.51°\text{C}, \theta = 27.18°$, are used to calculate that $I = 130 \pm 2\ \mu\text{Jm}$.

The theoretical and experimentally observed initial contact angles are displayed in Table 4.2.

Table 4.2: List of Initial Contact Angles of Water on Silicon

Experiment Name, Section #	Room Temp [°C]	Contact Angle [degrees]
Stored Water (1), 3.2.1	33.4	38.0
Stored Water (2), 3.2.1	26.9	23.0
New 17.5 MΩ-cm, 3.2.2	29.7	30.4
Standard Procedure, 3.2.3	29.7	22.6
Stored Water- Revisited, 3.2.4	24.4	31.9
Grounding the Cell(1), 3.2.5	34.0	23.7
Grounding the Cell(2), 3.2.5	27.5	22.6
Saltwater, 3.2.6	25.9	33.8
Charged Droplet, 3.2.7	22.4	30.2
Larger Droplet, 3.2.8	24.5	26.1
Average	27.8	28.2

Figure 4.2 shows a plot of all the experimental data. The sharp-kink approximation's prediction of the contact angle with I determined from information in Table 4.2 is displayed as an unbroken curve, while the I determined from T_w (discussed below) is displayed as a broken curve.

For the most part, the experimental contact angles are far greater than either theoretical curve predicts. One exception to this is the data from the experiment Grounding the Cell (1), which agree with the curve very nicely. Results from experiment Stored Water(1) is shown as an inset because the results from this experiment differed greatly from all other water on silicon results. Because it has a lower value of I, the predicted contact angle for water on silicon with I determined from T_w is always lower than that I determined from the initial contact angle.

Wetting Temperature determined I

Two experiments, one from Section 3.2.2 and one from Section 3.2.3, displayed evidence of a possible wetting transition. In Section 3.2.2 the wetting temperature was 44.5 °, and in Section 3.2.3 the wetting temperature was 45.0 °C. If

these were indeed wetting transitions, then Eq. 4.2 has a contact angle of 0 degrees, and becomes of the form

$$I = 2\frac{\sigma_{lg}}{\Delta\rho}(T_w) \tag{4.5}$$

Solving for I at the average wetting temperature of 44.75° determines

$$I = 133\mu\text{J m kg}^{-1} \tag{4.6}$$

4.1.3 Water on Gold

The contact angle of water on gold was measured because it was already known that $C = 19100 \pm 400$ KÅ^3 and $D = 1790 \pm 180$ K [31]. These values were used to calculate the van der Waals integral $I = 109\mu\text{J m kg}^{-1}$ and, in conjunction with the sharp-kink approximation, to predict wetting behavior and a wetting temperature for water on gold as a function of temperature.

Table 4.3 displays the initial contact angle of water on gold, both experimental observed, and theoretically determined

Table 4.3: List of Initial Contact Angles

Experiment Name, Section #	Temperature [°C]	Contact Angle [degrees]
Standard Procedure, 3.3	25.2	56.0
Theoretical Prediction From C, D	45.0	55.0

Figure 4.3 shows the contact angle of water on gold grew as temperature was increased from 25 to 102 °C. Temperature grew from 56 to 74 degrees over the temperature range. The predicted contact angle was always lower than the observed contact angle. Despite the apparent agreement at low contact temperature, observed contact angles disagreed with Eq. 4.1's prediction that the contact angle would monotonically decrease with temperature.

Since the water may have been charged later analysis examines the how electrostatic charging would effect the contact angle.

4.2 Experimental Deviation

The contact predicted using Eq. 4.1 monotonically decreases from its initial predicted value until the droplet undergoes a wetting transition. In almost every experiment, the observed initial contact angle was approximately equal to the predicted contact angle at room temperature, but as temperature increased so too did the deviation between observed contact angle and the predicted contact angle increase.

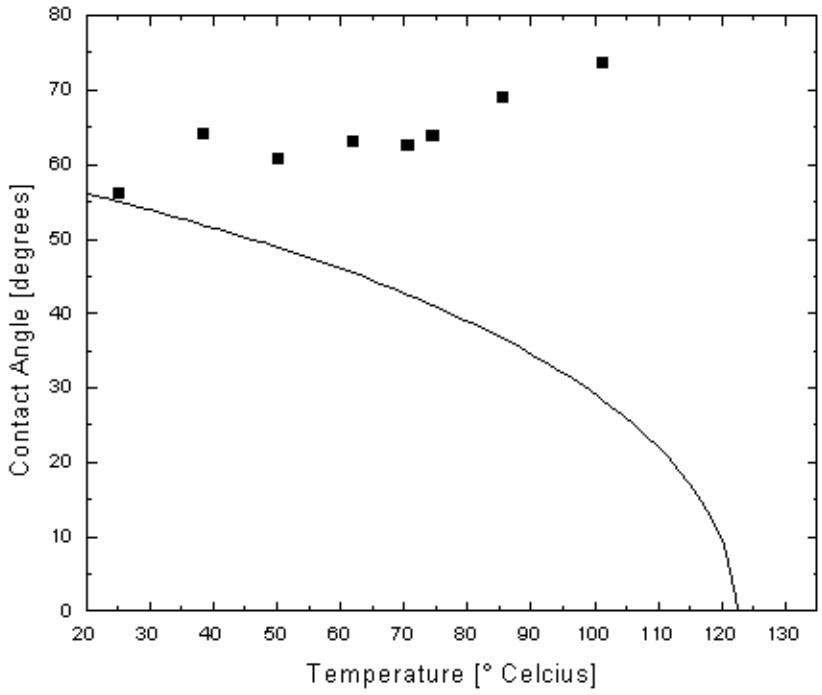

Figure 4.3: A plots of the theoretical and observed contact angle of water on gold. The theoretical curve is determined from the known van der Waals coefficients C and D [31] and the sharp-kink approximation.

In an attempt to understand the reason for the deviation between predicted and observed wetting tension, we made a correction to the sharp-kink approximation.

$$\sigma_{ls} \approx \sigma_{lg} + \sigma_{sg} - \Delta\rho\, I - H \tag{4.7}$$

Solving for H in terms of known quantities we have

$$H(T) = \sigma_{lg}(\cos\theta_{expt} - \cos\theta_{theory}) \tag{4.8}$$

Before we saw that the difference between the observed and predicted contact angles increased with T. $H(T)$ we expect to see decrease with increasing T because we are examining the difference of the cosine of the angles.

For most experiments, it was found that $H(T)$ was linear, *e.g.* of the form.

$$H(T) = mT + b \tag{4.9}$$

where T here is given in °C.

4.2.1 Deviations in Water on Graphite

Figure 4.4 shows plots of $H(T)$ for water on graphite, along with lines of best fit. The van der Waals integral I for water on silicon was calculated using C and D. As can be seen, the plots of Stored Water, and Increased Droplet Size (1) and (2) are linear over their range of experimentation. The H of the experiment New Water is not linear over the temperature range.

Table 4.4 shows the coefficients m, b that would be necessary to produce the lines in figure Figure 4.4. The results for New Water are not included in the table, because H was not seen to be linear in this experiment.

Table 4.4: Coefficients m and b from Eq. 4.7, Obtained from Experimental Data for Water on Graphite

Experiment Name	Slope, m J m^{-2} T^{-1} $\times 10^{-3}$	Intercept, b J m^{-2} $\times 10^{-3}$
Stored Water, 3.1.1	-0.15	-29.8
Increased Droplet Size (1), 3.1.3	-0.32	37.6
Increased Droplet Size (2), 3.1.3	0.26	-75.9

4.2.2 Deviations in Water on Silicon

Figure 4.5 shows the plots of H for the ten different experiments of water on silicon. H was linear for most experiments, and so lines of best fit for each water on silicon experiment were included in the plots. I was calculated using the initial contact angle data and Eq. 4.2. In several of the experiments there weren't many data points below the theoretical wetting temperature. This resulted in a several linear regressions based on only three or four data points, shedding doubt on the linearity of equation.

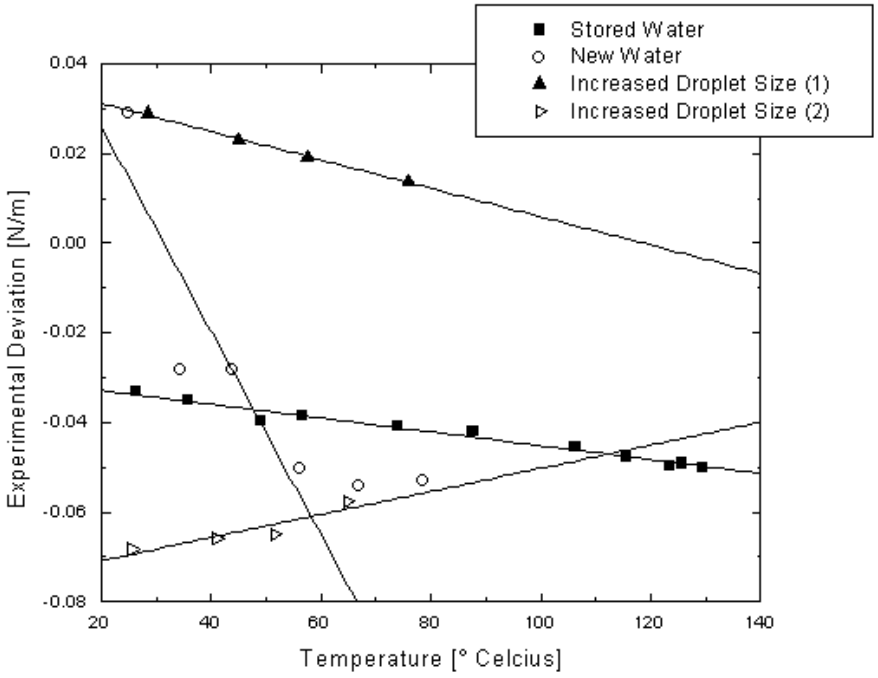

Figure 4.4: The plots of each experiment's results for Eq. 4.8 of water on graphite. The experiment New Water is the only experiment that appears non-linear. The experiment named 'Stored Water' used 17.5 MΩ-cm water, while all others used 18.2MΩ-cm

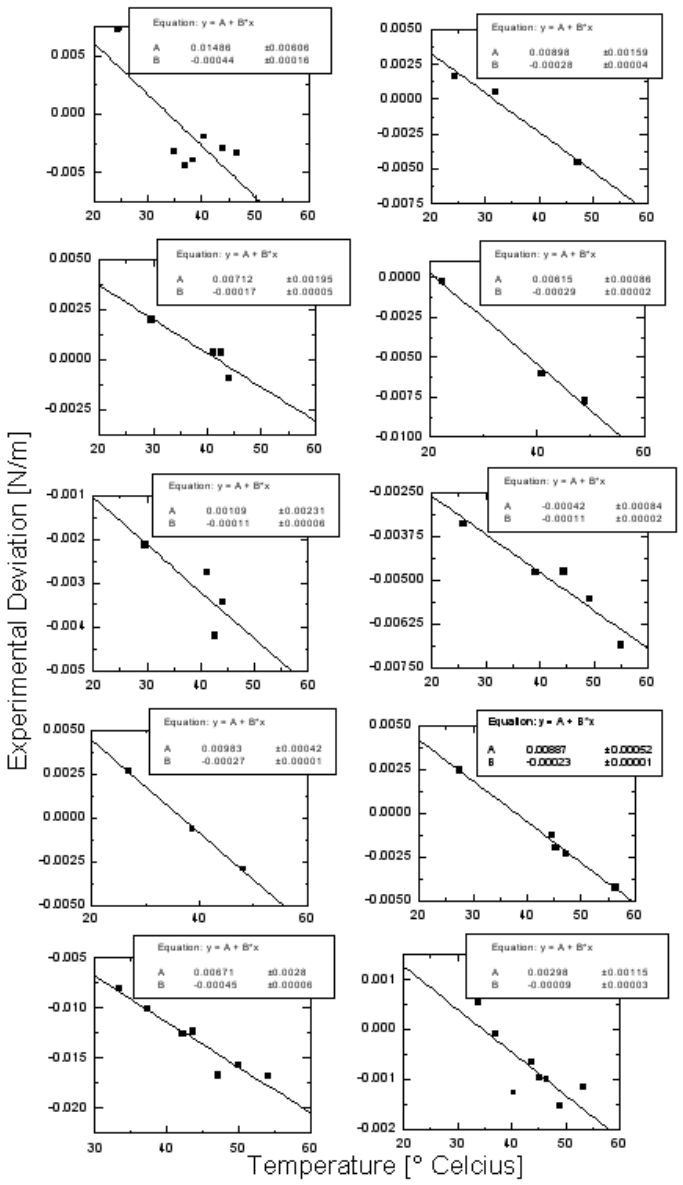

Figure 4.5: The plots of $H(T)$ from Eq. 4.8 of water on silicon for most experiments. In several of the experiments there weren't many data points below the theoretical wetting temperature, which shed doubt on the linearity of equation.

Table 4.5 shows the coefficients m, b that would be necessary to produce the lines in Figure 4.5.

Table 4.5: Coefficients m and b from Eq. 4.7, Obtained from Experimental Data for Water on Silicon

Experiment Name, Section #	Slope, m J m^{-2} T^{-1} $\times 10^{-3}$	Intercept, b J m^{-2} $\times 10^{-3}$
Stored Water (1), 3.2.1	-0.45	6.7
Stored Water (2), 3.2.1	-0.27	9.8
New 17.5 MΩ-cm, 3.2.2	-0.11	1.1
Standard Procedure, 3.2.3	-0.17	7.1
Stored Water- Revisited, 3.2.4	-0.44	14.9
Grounding the Cell(1), 3.2.5	-0.09	3.0
Grounding the Cell(2), 3.2.5	-0.23	8.9
Saltwater, 3.2.6	-0.11	-0.4
Charge Droplet, 3.2.7	-0.29	6.2
Larger Droplet, 3.2.8	-0.28	9.0

The data from the individual experiments are plotted together in Figure 4.6. When seen together, it is more convincing that the experimental deviation is linear, because it demonstrates that deviations are all approximately equal in magnitude.

The experiment Stored Water (1), as was mentioned before, was an outlier in that contact angle was observed to increase with temperature. Here again Stored Water (1) is an outlier, having a greater negative slope than the rest of the experiments. Furthermore, the H for Stored Water (1) has a very low χ^2 per degree of freedom, and many data points. This shows that Stored Water (1) is linear despite being an outlier.

Based on all the individual deviations, a visual average was used to determine the average deviation. The average deviation does not take into account the outlier H.

$$H(T) = (1.3 \pm 2.1) \times 10^{-4}\, T + (-1 \pm 4) \times 10^{-4} \tag{4.10}$$

4.2.3 Water on Gold

We calculated the experimental deviation H from theory for water on gold using van der Waals coefficients C and D. Figure 4.7 shows the plot of H for water on gold along with a line of best fit. H decreases linearly with increasing temperature, with a 95 % confidence level.

Table 4.6 shows the coefficients m, b that would be necessary to produce the lines in Figure 4.7.

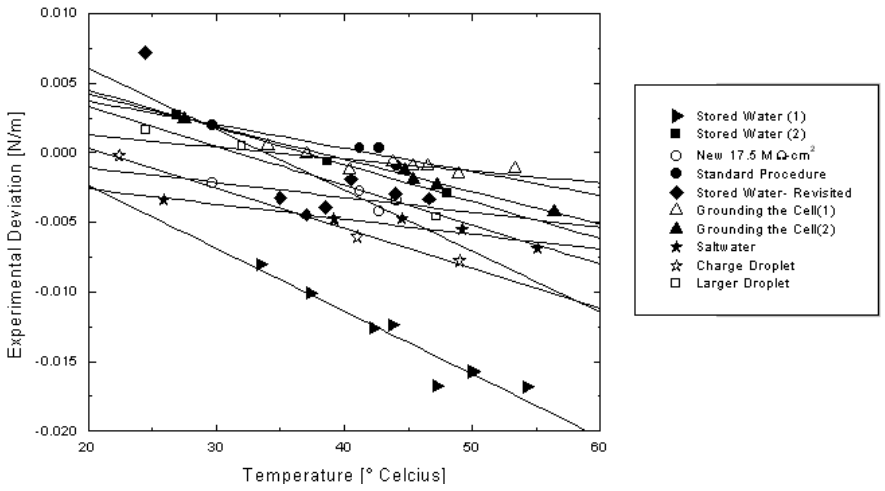

Figure 4.6: The plots of $H(T)$ from Eq. 4.8 of water on silicon all on one graph. The data from $H(T)$ are very close to one another over this region. Different conditions are explained in Table 4.5.

Table 4.6: Coefficients m and b from Eq. 4.7, Obtained from Experimental Data for Water on Gold

Experiment Name	Slope, m J m^{-2} T^{-1} $\times 10^{-3}$	Intercept, b J m^{-2} $\times 10^{-3}$
Standard Procedure	-0.37 $\pm$ 0.04	7 $\pm$ 3

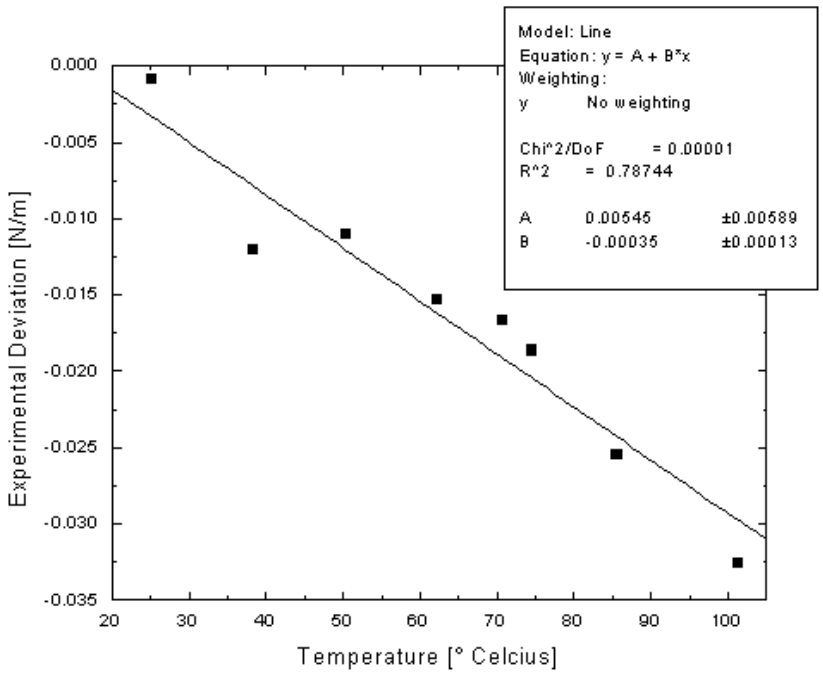

Figure 4.7: The plots of $H(T)$ from Eq. 4.8 of water on gold form a line.

4.3 Sources of Error

As we have seen, observed contact angles were higher than predicted contact angles, with few exceptions. These experimental deviations might be due to several factors including temperature gradients, pinning, chemical reactions and electrostatic charging effects. Electrostatic charging effects are discussed in detail in the next section.

4.3.1 Temperature Gradients

Temperature gradients between the thermometer on the outside of the cell and the temperature inside the cell provide a possible explanation for the apparently low theoretical contact angle prediction. It was impossible to cleanly put the thermometer in the cell to more precisely measure the droplet temperature. Since the experiments were done with the temperature increasing, the temperature inside the cell can be expected to have always lagged lower than the temperature outside. This would lead us to expect that the observed contact angle would be higher than the predicted contact angle. However, such temperature gradients cannot be the sole source of this error because when the temperature stopped increasing the contact angle did not agree with the theory better.

Within the cell there were also temperature gradients caused by non-uniform thermal insulation around the cell. The temperature of the air near the windows was the biggest source of internal temperature gradients. We suspect internal temperature gradients to be forming near windows, because water condensed onto the edge of the substrate nearest to the window. These temperature gradients in the cell weren't controlled nor were they calculable. Although an effort was made to minimize internal gradients, it is unclear how well these methods worked. It is unclear how internal gradients would effect observed contact angles.

4.3.2 Adsorption of Water onto Substrate

At the beginning of each experiment, at most a thin layer of water was supposed to adsorb onto the substrate for Eq. 4.1 to be valid. This adsorbate layer is supposed to be a negligibly thick, and present everywhere on the substrate. To promote adsorption, the substrate and a reservoir of water were sealed in the cell for up to twenty minutes before placing the droplet on the substrate. Although the reservoir and sample were allowed to equilibrate before the droplet was inserted into the cell, this equilibration might have been compromised when the cell was reopened to insert the droplet.

It was also possible that if the droplet did adsorb onto the substrate, the water could form a layer of non-neglible thickness. In such instances, Eq. 4.1 is not valid and it is not clear how we could correct for this effect.

4.3.3 Pinning

Pinning, due to impurities on the surfaces and in the water could cause contact angle to differ from the theoretically predicted angle. Pinning acts as a frictional force,that would act to hold the contact line in place on the substrate. Since the observed contact angle often lagged behind the predicted contact angle, it may be hypothesized that pinning led to this error. Furthermore, it is possible that during the silicon experiments several of the droplets were pinned on the surface at the beginning of the experiment. This would account for the several experiments in which the contact angle changed very little.

However, further analysis suggests that pinning may not have been responsible for the observed contact angle behavior. There were several experiments where the droplet volume decreased in contact angle. If evaporation occurred uniformly over the surface of the exposed droplet, decreasing the volume and the the contact line were pinned, then the droplet would have a lower contact angle when temperature was increased. However, we saw that as temperature increased, contact angle also increased, which is seems to contradict the assumption that the contact angle was pinned.

4.3.4 Chemical Reactions

Another effect that should be considered is that the water in the cell might have reacted with the stainless steel, introducing impurities into the atmosphere within the cell. On a similar note, droplet water could be reacting with graphite, although this is unlikely because graphite is not very reactive. It is uncertain how such reactions would affect observed contact angles.

As is mentioned at the beginning of the discussion section, electrostatic effects cold be causing some source of error, and this source of error is modeled in the discussion. The stored 17.5 MΩ-cm water may have been charged if its plastic storage container was charged, and the 18.2 MΩ-cm water might have become charged in the filtering process. Several pages are devoted to determining the impact of electrostatic charging in the discussion section above.

4.4 Interface Charging

If the interface ever became charged, either due to a chemical reaction or because the droplet was charged and the interface responded, then the sharp-kink approximation needs to be corrected to take the charging into account. Kang *et al* [28] determined that corrections should be of the form $H(T)$. In this case, the sharp-kink approximation becomes

$$\cos\,\theta = -1 + \frac{\Delta\rho}{\sigma_{lg}} I + \frac{1}{\sigma_{lg}} H \tag{4.11}$$

.

In the case of a stoichiometrically balanced z:z electrolyte in a droplet of constant charge, Kang *et al* [28] determined $H(T)$. Figure 4.10 contains a

diagram, and a description of $H(T)$.

$$\begin{aligned} H = \quad & \left\{ 8\frac{n_1 kT}{\kappa_1}\left[\cosh\ \frac{\beta\psi_{1\infty}}{2} - 1\right] - \Sigma_1\psi_{1\infty}\right\} \\ & - \left\{ 8\frac{n_2 kT}{\kappa_2}\left[\cosh\ \frac{\beta\psi_{2\infty}}{2} - 1\right] - \Sigma_2\psi_{2\infty}\right\} \\ & + (\Sigma_1 - \Sigma_2)\psi_0 \end{aligned} \tag{4.12}$$

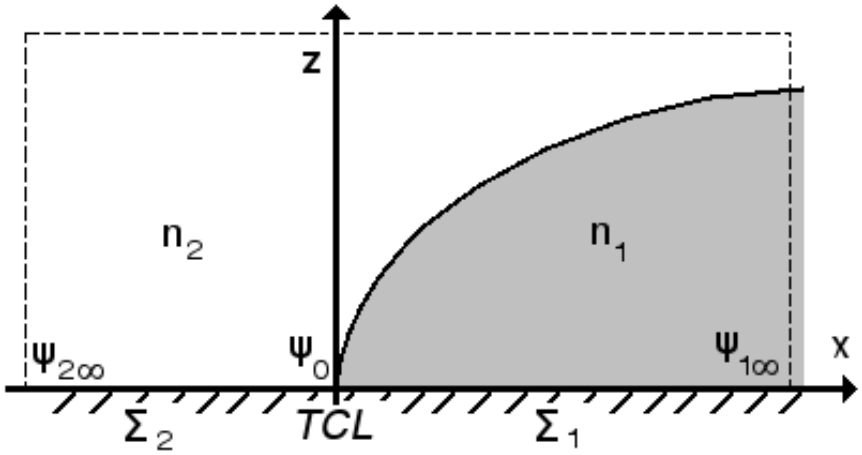

Figure 4.8: Here n_i are the ion concentrations, $\psi_{i\infty}$ is the electric potential far from the TCL in medium i, the κ_i are the Debye lengths, and $i = 1, 2$ for in the bulk water and air surrounding the droplet, respectively. Σ_1, Σ_2 are the coulombic surface charge densities exposed to the bulk, and exposed to the open air, respectively. Furthermore the constants κ and β are given in terms of the z the valency of the ionic species, and ϵ the permittivity of water in Eq. 4.13.

$$\kappa = \left(2nz^2e^2/\epsilon kT\right)^{1/2} \qquad \beta = \frac{ze}{kT} \tag{4.13}$$

We assume that during our experiments $n_2 = 0$, which means that

$$H = 8\frac{n_1 kT}{\kappa_1}\left[\cosh\ \frac{\beta\psi_{1\infty}}{2} - 1\right] + \Sigma_2(\psi_{2\infty} - \psi_0) - \Sigma_1(\psi_{1\infty} - \psi_0) \tag{4.14}$$

Thus if droplet charging can be modeled by Kang's formula, then the deviation function $H(T)$ is of the form

$$\begin{aligned} H(T) &= \sigma_{lg}\left[cos\,\theta_{exp} - \cos\ \theta_{ideal}\right] \\ &= A\left(\psi_\infty, n, T\right) + \Sigma_2(\psi_{2\infty} - \psi_0) - \Sigma_1(\psi_{1\infty} - \psi_0) \end{aligned} \tag{4.15}$$

Where, for brevity, we write

$$A\left(\psi_{\infty}, n, T\right) = \frac{8nkT}{\kappa}\left[\cosh\ \frac{\beta\psi_{\infty}}{2} - 1\right] \tag{4.16}$$

The osmotic pressure caused by charges in a droplet was calculated by Israelachvili [8]. The osmotic pressure will be useful because it is related to A and can be used to generalize Kang's equation.

$$\Pi = kT\left[n_1\left(exp(\beta_1\psi_m) - 1\right) + n_2\left(exp(\beta_2\psi_m) - 1\right)\right] \tag{4.17}$$

where $\psi_m = \psi_{i\infty}/2$ and is the electric potential at the mid-plane.

For a z:z electrolyte, Kang found that [28]

$$\Pi = nkT\left[(exp(-\beta\psi_m) - 1) + (exp(\beta\psi_m) - 1)\right] \tag{4.18}$$

$$\Pi = 2nkT\left[\cosh\ \beta\psi_m - 1\right] \tag{4.19}$$

We see that the first term in $H(T)$ is related to the osmotic pressure at the mid-plane Π in the following manner.

$$\Pi = \frac{\kappa}{4}A\left(\psi_{\infty}, n, T\right) \tag{4.20}$$

Thus if we know the osmotic pressure, we know A. As such, we can calculate the A for non z:z electrolytes by determining Π

4.4.1 A Simple Estimate of the Electrostatic Forces

In light of such predictions, it follows that the difference in observed and calculated wetting tensions is given by Eq. 4.15. In all but one case, the deviation function $H(T)$ decreased with increasing temperature. Thus one of the terms in Eq. 4.14 must negative if electrostatic charging is causing the decreased contact angle.

Does A Decrease as T Increases?

In an attempt to explain the behavior of the contact angle, we shall first determine the plausibility of linear discrepancy with Eq. 4.1 being due to the temperature-dependence of $A(T)$. The possible effect of the temperature-dependence of $\Sigma_1(\psi_{\infty} - \psi_0) + \Sigma_2(\psi_{\infty} - \psi_0)$ will be considered below.

First we examine the case of the z:z electrolyte

$$A\left(\psi_{\infty}, n, T\right) = \frac{8nkT}{\kappa}\left[\cosh\ \frac{\beta\psi_{\infty}}{2} - 1\right] \tag{4.21}$$

For any argument x of cosh x yields a number greater than unity. As such, $\left[\cosh\ \frac{\beta\psi_{\infty}}{2} - 1\right]$ must be positive. Likewise the concentration n and Debye length κ are defined to be positive quantities. Temperature is reported in Kelvin,

and the experiment see no nonnegative temperatures. Therefore it must be that for a z:z electrolyte, A is positive.

In general, any neutral molecules species that dissociates into two different species in the water are of the form $|z_1 n_1| = |z_2 n_2|$. Thus we can write the osmotic pressure caused by such molecules as

$$\Pi = n_1 kT \left[\left(exp \frac{z_1 e \psi_m}{kT} - 1 \right) + \left| \frac{z_1}{z_2} \right| \left(exp \frac{z_2 e \psi_m}{kT} - 1 \right) \right] \tag{4.22}$$

It can be shown that for any integer choice of z_1, z_2 that $\Pi > 0$. Since $A \propto \Pi$ we get A is positive, and thus A is not capable of causing the decreasing $H(T)$ observed in experiments.

Temperature-Dependence of Electric Surface-Energies

Since the temperature-dependence of $A(T)$ cannot account for decreasing $H(T)$, we also consider the possible affect of electric surface-energies are of the form

$$H = \Sigma_2(\psi_{2\infty} - \psi_0) - \Sigma_1(\psi_{1\infty} - \psi_0) \tag{4.23}$$

If the substrate were charged in our experiment, then we see that Σ_2 and $\psi_{2\infty}$ should be constant because the droplet is small compared with the substrate. Thus Eq. 4.23 allows for contribution to either wetting or non-wetting depending on the behavior of $\Sigma_1, \psi_{1\infty} - \psi_0$, and ψ_0, as described below.

First let's consider the case where the Electric Potential between the center of the droplet and the three phase contact line is constant shown, see Figure **??**. As temperature increases, the droplet spreads. Which means that the distance between $\psi_{1\infty}$ and ψ_0 grows as temperature increases. In this case, the charge on in the droplet constant as the surface area grows, which means that Σ_1, the charge per area, must decrease as temperature increases. A decreasing H contributes to wetting as T increases.

Next, let's consider the case where Σ_1 is constant, see Figure **??**. Again, the distance between $\psi_{1\infty}$ and ψ_0 grows as temperature increases. Because Σ_1 is constant, the electric field over a larger distance causes a greater potential difference between the TCL and the center of the droplet. Thus as T grew the potential difference $\psi_{1\infty} - \psi_0$ would also grow. An increase H contributes to non-wetting behavior.

Furthermore when H increases with temperature $H(T)$ decreases with temperature. Since a decreasing $H(T)$ was observed, it is possible that temperature dependent electric surface-energies caused the observed experimental deviation.

4.5 Conclusions

The main result of experimentation is that the ideal sharp-kink approximation does not describe the temperature-dependence for the contact angle of water on various substrates if only van der Waals forces are taken into account in Eq. 4.1.

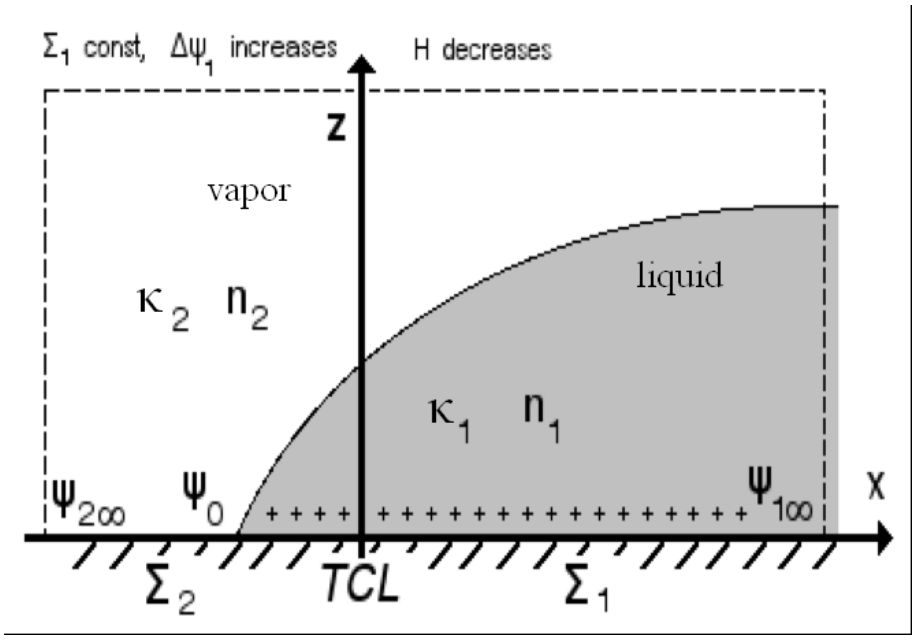

Figure 4.9: A droplet on a substrate that has constant Σ_1. The droplet spreads with increasing temperature. As the droplet spreads past the old TCL the horizontal electric field on the substrate increases, which means that H decreases.

Table 4.7: Theoretical and Experimental Values I.

Substrate Material	Experiment or Theory	I μ J m kg^{-1}	δI μ J m kg^{-1}
Graphite	Theory	71.5	0.4
Graphite	ICA	64.4	10.1
Silicon	ICA	13.3	2
Silicon	Wetting Temp	13	1
Gold	Theory	109.30	0.01

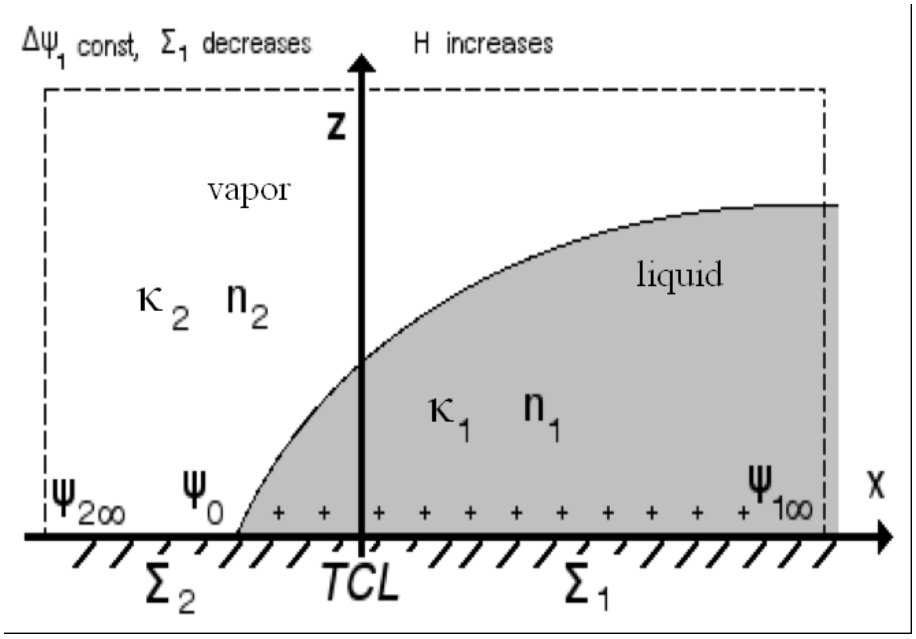

Figure 4.10: A droplet on a substrate that has constant $\psi_{1\infty} - \psi_0$. The droplet spreads with increasing temperature. As the droplet spreads past the old TCL the horizontal electric field on the substrate decreases, which means that H increases.

This is surprising because it means that more forces than just van der Waals are major players in the wetting of water at room temperature.

The contact angle of water on various substrates did not monotonically decrease in every experiment as predicted by the ideal sharp-kink approximation, given by Eq. 4.1. Instead, a variety of behaviors were observed, including monotonic decrease of contact angle, no change in contact angle, and increase in contact angle, some of which would be impossible according to Eq. 4.1.

To a first approximation at room temperature, the sharp-kink approximation correctly predicted angle the contact angle, for water on graphite and gold. However for water on graphite, the sharp-kink approximation deviated from observed contact angles by no more than 30 degrees. Table 4.8 shows the observed and predicted initial contact angles and temperatures.

Table 4.8: Initial Contact Angles Compared with Contact Angles Given by Eq. 4.1.

Data Set	T_0 [°C]	δT	θ_0 [degrees]	$\delta\theta$
Graphite-Avg	26.4	1.6	95.8	14.0
Graphite-Using C and D	26.5		88.2	
Si-Avg	28.5	3.8	27.2	5.6
Si-Using Initial Contact Angle	28.3		27.5	
Gold	25.2		56.0	0.5
Gold-Using C and D	25.6		54.8	

We found that deviations from predicted temperature-dependence was distinctly linear and decreasing in temperature, although some data sets had too few points to show linearity.

Our analysis showed Section 4.4.1 that electrostatic charging effects can possibly account for this linear discrepancy although entropic double-layer forces cannot. More experimentation is necessary to confirm this.

4.6 Suggestions for Further Work

Beyond the scope of this paper are some points of further interest.

Analyzing the water used in the three experiments that demonstrated an increase in contact angle would help us to determine if the water caused the anomalous contact angle behavior.

Additional experiments would determine whether this paper's observed contact angle behavior of water on gold was anomalous, and would help future experimenters determine the proper question, either: "Why does water's contact angle on gold grow with increasing temperature?" or "Why did water's contact angle on water grow with increasing temperature during this experiment?"

Removing the temperature gradients would allow for more accuracy and precision in experimental results. The error due to temperature gradients could re-

moved by placing a thermometer within the cell. Temperature gradients within the cell could be controlled by designing a cell that had the same heat flux through the windows as through the cell body.

Experiments that examined the adsorbate layer of water on the substrate via ellipsometry before and during experimentation would be useful. Such measurements would tell the film thickness at any given location on the substrate, and eliminate uncertainties about the adsorbate layer.

Bibliography

[1] Cahn, J. W.; *J. Phys. Chem.* **1977**, 66, 3667; Ebner, C.; Saam, W. F.; *Phys. Rev. Lett.* **1977**, 38, 1486; Bonn, D.; Ross, D.; *Rep. Prog. Phys.* **2001**, 46, 1085; Hallock, R. B.; *J. Low Temp. Phys.* **1995**, 101 31; de Gennes, P. G.; *Rev. Mod. Phys.* **1985**, 57, 827.

[2] Ancilotto, F.; Curtarolo, S.; Toigo, F.; Cole, M. W.; *Phys. Rev. Lett.* **2001**, 87, 206103; Hess, G. B.; Sabatini, M. J.; Chan, M. H. W.; *Phys. Rev. Lett.* **1997**, 78, 1739; Cheng, E.; Mistura, G.; Lee, H. C.; Chan, M. H. W.; Cole, M. W.; Carraro, C.; Saam, W. F.; Toigo, F.; *Phys. Rev. Lett.* **1993**, 70, 1854; Taborek, P.; Rutledge, J. E.; *Phys. Rev. Lett.* **1992**, 68, 2184; J.E. Rutledge and P. Taborek, *Phys. Rev. Lett.* **1992**, 69, 937; Ketola, K. S.; Wang, S.; Hallock, R. B.; *Phys. Rev. Lett.* **1992**, 68, 201; Nacher, P. J.; Dupont-Roc, J.; *Phys. Rev. Lett.* **1991**, 67, 2966.

[3] Kruchten, F.; Knorr, K.; *Phys. Rev. Lett.* **2003**, 91, 085502.

[4] Ross, D.; Rutledge, J. R.; Taborek, P.; *Science* **1997**, 278, 664; Ross, D.; Taborek,P.; Rutledge, J. R.; *J. Low Temp. Phys.* **1998**, 111, 1; Rutledge, J. R.; Ross, D.; Taborek,P.; *J. Low Temp. Phys.* **1998**, 113, 811.

[5] Klier,J. ; Stefanyi, P.; Wyatt, A. F. G.; *Phys. Rev. Lett.* **1995**, 75, 3709; Klier, J.; Leiderer, P.; Reinelt, D.; Wyatt, A. F. G.; *Phys. Rev. B* **2005**, 72, 245410.

[6] Ross, D.; Taborek, P.; Rutledge, J. E.; *Phys Rev. B.* **1998**, 58, R4274.

[7] Young, T.; *Philos. Trans. R. Soc. London* **1865**, 95, 65.

[8] Pashley, R. M.; Israelachvili, J. N.; *Colloids Surf.* **1981**, 2, 169; Israelachvili, J. N.; *Adv. Colloid Interface Sci.* **1982**, 16, 31; as cited in: Israelachvili, J. N.; *Intermolecular and Surface Forces, 2nd Ed.*; Elsevier Ltd: London, 1992, p.322.

[9] Dietrich, S.; Schick, M.; *Phys. Rev. B* **1986**, 33, 4952; Dietrich, S.; Napiórkowski, M.; *Phys. Rev. A* **1991**, 43, 1861; Dietrich, S.; in *Phase Transitions and Critical Phenomena*, Domb, C.; Lebowitz, J. L., eds.; Academic: London, 1988, Vol. 12, p. 1.

[10] Heine, D. R.; Grest,G. S.; Webb III, E. B.; *Phys. Rev. E* **2003**, 68, 061603; Heine, D. R.; Grest, G. S.; Webb III, E. B.; *Phys. Rev. E* **2004**, 70, 011606.

[11] Ancilotto, F.; Sartori, A. M.; Toigo, F.; *Phys. Rev. B* **1998**, 58, 5085.

[12] Cheng, E.; Cole, M. W.; Saam,W. F.; Treiner, J.; *Phys. Rev. Lett.* **1991**, 67, 1007 and *Phys. Rev. B* **1992**, 46, 13967; Cheng, E.; Cole, M. W.; Dupont-Roc, J.; Saam,W. F.; Treiner, J.; *Rev. Mod. Phys.* **1993**, 65, 557; Ebner, C.; Saam,W. F.; *Phys. Rev. Lett.* **1971**, 38, 1486; Finn,J. E.; Monson, P. A.; *Phys. Rev. A* **1989**, 39, 6402.

[13] Chizmeshya, A.; Cole, M. W.; Zaremba, E.; *J. Low Temp. Phys.* **1998**, 110, 677.

[14] E.g., Adamson, A. W.; Gast,A. P.; *Physical Chemistry of Surfaces, Sixth Ed.,* John Wiley and Sons, 1997, Section X.7.

[15] Gatica, M.; Zhao, X.; Johnson, J. K.; Cole, M. W.; *J. Phys. Chem. B* **2004**, 108, 11704.

[16] Zhao, X.; Johnson, J. K.; *Molecular Simulation* **2005**, 31, 1.

[17] Werder, T.; Walther, J. H.; Jaffe, R. L.; Halicioglu, T.; Koumoutsakos,P. J.; *Phys. Chem B* **2004**, 107, 1357; Pertsin, A.; Grunze, M. J.; *J. Phys. Chem. B* **2004**, 108, 1557.

[18] Schrader, M. E.; *J. Phys. Chem.* **1980**, 84, 2774.

[19] Ponter, A. B.; Yekta-Fard, M.; *Colloid and Polymer Sci.* **1985** 263, 673.

[20] ZYA grade Pyrolytic Graphite Monochromator, GE Advanced Ceramics.

[21] Fowkes, F. M.; Harkins,W. D.; *J. Am. Chem. Soc.* **1940**, 62, 3377.

[22] Morcos, J.; *J. Chem. Phys.* **1972**, 57, 1801.

[23] Plaksin, I. N.; Bessonov, B. V.; *Dokl. Akad. Nauk SSSR* **1948**, 61, 865.

[24] White, M. L.; *J. Phys. Chem.* **1964**, 68, 3083.

[25] Erb, R. A.; *J. Phys. Chem.* **1968**, 72, 2412.

[26] Kwok, D. Y.; Li, D.; Neumann, A. W.; *Langmuir* **1994**, 10, 1323; D. Li A. W. Neumann, *J. Colloid Interface Sci.* **1992**, 148, 190.

[27] Langmuir, I.; *J. Chem. Phys.* **1938** 6, 873.

[28] Kang, K. H.; Kang, I. S.; Lee, C. M.; *Langmuir* **2003**, 19, 5407; Chou, T.; *Phys. Rev. Lett.* **2001**, 87, 106101.

[29] Yaminski, V. V.; Johnston, M. B.; *Langmuir* **1995**, 11, 4153.

[30] Youn, H. S.; Meng, X.F.; Hess, G. B.; *Phys. Rev. B* **1993** 48, 14556; P. Müller-Buschbaum, *Eur. Phys. J. E* **2003**, 12, 443.

[31] Garcia, R.; Subashi, E.; Osborne, K.; *J Phys Chem B* **2008** 112, 8114.